land

MDPI

Article

Heat as a Located Constraint on Grain Production in a Humid Basin: Implications for Climate-Adaptive Land Management

Xu Lin [1], Yanbin Qi [1,*] and Qiang He [2]

[1] College of Economics, Sichuan Agricultural University, Chengdu 610030, China; 2026108008@stu.sicau.edu.cn
[2] School of Management, Yunnan Normal University, Kunming 650031, China
* Correspondence: qybin@sicau.edu.cn

Abstract

In humid agricultural regions, where heat and water deficit are decoupled, temperature acts on crops in two opposed ways: moderate warmth advances development, whereas extreme heat damages it, and land management must distinguish them. This study examined the temperature response of grain production in the Sichuan Basin, southwestern China, and translated it into priorities for climate-adaptive land management. Growing degree days (GDDs) and extreme degree days above 30 °C (EDD30s) were built from gridded daily mean temperature; the response was estimated for 183 county-level land units over 2014–2024 with two-way fixed-effects models and full controls. July and August constitute the critical growth period; the findings are fourfold. (1) Over this window, 100 additional GDDs raised grain yield by 2.70% and 100 additional EDD30s lowered it by 3.24%. (2) Damage deepened as the threshold rose, from 2.52% at 30 °C to 10.23% at 34 °C per 100 degree-days, while coarse indices carried no signal. (3) The constraint centred on July, persisted under spatial inference at all bandwidths, and was not moderated by irrigation. (4) A total of 67 of the 177 estimation counties combined above-median exposure with above-median output, producing 69.6% of basin grain. The results point to a direct thermal channel rather than water deficit, supporting adjustments to cropping calendars and cultivar choice rather than irrigation expansion in the eastern plain.

Keywords: high temperature; heat damage; humid cropland; land; grain production; Sichuan Basin

1. Introduction

Cropland is the part of the land surface that converts climate variability most directly into food production. Extreme heat has become the dominant climatic threat to that conversion [1,2], and the pressure it places on land systems extends well beyond food production [3]. The 2022 drought and heat wave across the Yangtze River basin was the most severe on record, and it depressed vegetation productivity across a region that supplies a large share of China's grain [4]. Heat enters the land system as a spatially and temporally concentrated stressor, not as a uniform background condition. Its consequences depend on where cropland sits in the landscape, when the sensitive phenological stages occur, and how water and land are managed around them [5,6]. Two properties of the temperature signal are frequently conflated. Moderate warmth accumulated over a growing season is a resource that advances development, whereas heat above a physiological threshold is a stressor that shortens grain filling, depresses photosynthesis, and increases respiratory losses [7,8]. Because the two are positively correlated across years, an index built from

Check for updates

Academic Editors: Mohamed A. Mattar and Ali Salem

Received: 2 October 2026
Revised: 12 October 2026
Accepted: 14 October 2026
Published: 15 October 2026

Copyright: © 2026 by the authors. Licensee MDPI, Basel, Switzerland. This article is an open access article distributed under the terms and conditions of the Creative Commons Attribution (CC BY) license.

mean temperature or from a low degree-day base captures both at once, and the estimated effect becomes an artefact of whichever component dominates the sample. Land-based assessments that intend to inform adaptation must therefore separate the two before drawing any management conclusion [9,10].

This distinction is not semantic, because the two candidate damage channels imply opposite land-management responses. If heat damages crops mainly by aggravating water deficit, the constraint is hydrological. The appropriate instruments are then irrigation, terracing, mulching, and drainage. If heat acts directly on the plant, water-based interventions cannot relax the constraint. Adaptation must then operate through the cropping calendar, the cropping structure, and the heat tolerance of the varieties planted [11,12]. Most of the evidence on this choice comes from arid and semi-arid rainfed systems, where high temperature and water deficit are strongly collinear and hot years are dry years. In those settings, it is difficult to attribute observed damage to either stress alone [13,14]. The protective role of irrigation also appears unambiguous, and the proposition that heat acts through drought is difficult to falsify, even though temperature and humidity interact in ways that amplify losses where rainfall is adequate [15]. Humid croplands relax that constraint. Where rainfall exceeds crop water demand in most years, and the irrigated share of cropland is already high, heat damage that persists cannot be attributed to water deficit. Heat damage that disappears, by contrast, would show that the temperature–yield relationship estimated in dry regions does not generalise. A similar question is not confined to a single basin. Humid subtropical and monsoon croplands cover much of southern China, Southeast Asia, the Ganges–Brahmaputra plain, and parts of Latin America. They are typically managed intensively, with high inputs and little fallow, so that a biophysical constraint translates rapidly into production losses [16,17], and recent work in the humid subtropics of southern China shows that growth-stage-specific concurrent extremes are already detectable in rice yields [18].

A large body of econometric work has established that the temperature–yield relationship is strongly nonlinear. Its shape depends on how exposure is measured. For United States maize, soybean, and cotton, yields have been shown to rise with temperature up to roughly 29–32 °C and to fall sharply beyond it [13]. A comparable nonlinearity has been documented in aggregate economic output [19], and the agronomic basis for degree-day measures over mean temperature has been formalised [20]. The same pattern has been recovered for global crop production [21,22] and for Chinese county-level yields [23], where the estimated response differs across rice types [24]. It also holds for wheat in multi-model ensembles [25] and for African maize in historical variety trials and subsequent farm surveys [14,26]. Parallel work links temperature shocks to agricultural output and economic growth [27,28] and to the incidence of conflict [29]. Three limitations recur. First, the choice of a high-temperature threshold is rarely tested against alternatives, although it determines both the estimated magnitude and the interpretation of the result [20,30]; recent hemispheric evidence shows that the threshold at which heat becomes damaging is itself geographically heterogeneous [31]. Second, coarse climatic indices derived from low degree-day bases or percentile thresholds are widely used in land suitability and land capability mapping, although they carry little information about absolute heat stress [32,33]. Third, heat exposure is spatially clustered, so residuals of land-productivity models are frequently spatially correlated and conventional cluster-robust standard errors can then be too small [34–36]. A defensible estimate therefore needs an explicit threshold test, a comparison against the coarse indices actually used in land evaluation, and inference that survives spatial dependence.

For this test, the humid Sichuan Basin in southwestern China provides a strong setting. The basin floor is one of the most heat-prone agricultural regions in the country. It has

a humid subtropical climate, an irrigated share of cropland above one half, and a rice–rapeseed and maize–rapeseed cropping system whose critical growth stages fall in July and August. Mid-summer heat waves associated with the western Pacific subtropical high are a recurring hazard and have been intensifying [37,38]. The basin also experienced record-breaking heat and drought in August 2022 and again in 2024. Because water is not the binding constraint in most years, the basin separates the two damage channels that are entangled elsewhere. Recent work in the region documents northward shifts in climatic zones [39], changes in climate potential productivity [33], and a coupling between climate and cropland that runs through human activity [40]. Related studies report the sensitivity of cropland productivity to flash drought [41] and heterogeneous yield responses to planting-structure change [42]. The spatial heterogeneity of Chinese crop-yield responses to the environment has also been documented [23]. Land-system research has examined how land-management change functions as adaptation [12,43], and how sustainable land management is implemented under climatic stress [44]. Two strands of that work are directly relevant here: cropland adjustment as a response to climate shocks [45], and the spatial prioritisation of land and water management measures [46]. These contributions establish the regional context. They differ, however, in extent, period, exposure definition, and land classification, which limits direct comparison of the estimated heat response.

The gap is therefore substantive rather than technical. In humid croplands, heat and water stress are decoupled, so neither a threshold estimated in dryland settings nor the policy prescriptions built on it can simply be transferred. No study known to the authors has nevertheless done three things at once in such a setting: located the threshold against a full set of alternatives, treated the spatial dependence of the resulting residuals as a property to be measured rather than assumed away, and followed the heat signal through the land-use margin to total output. This paper does all three for one of the most heat-exposed humid grain systems in China. Table S1 sets the ten closest regional studies against this paper along setting, exposure definition, outcome, and land-use margin, and records for each what it leaves aside, so that the three elements claimed here can be checked against the existing evidence rather than asserted. The three elements are placed within a single county-level land-system framework: the full temperature–response function is recovered and its threshold is tested against the coarse indices used in land evaluation; the spatial dependence of the estimated residuals is quantified and accommodated; and the heat signal is followed through land use to output and to yield volatility, so that the food-security reading of the result does not rest on yield alone.

On the basis of the environmental and management contrasts of the basin, four outcomes were expected. First, the analysis anticipated a nonlinear temperature–yield relationship within the July–August critical growth period, with moderate warmth beneficial and heat above a threshold damaging. The threshold located here should be comparable to the 29–34 °C range used in the crop-yield literature, once daily mean and daily maximum temperature are placed on a common footing. Second, coarse measures based on an 18 °C base, on annual mean temperature, or on percentile exceedance were expected to carry little information about crop heat damage. Damage was anticipated to deepen monotonically as the threshold was raised, at the cost of thinner statistical support. Third, heat exposure and grain production were expected to be spatially concentrated in the same part of the basin, so that a small number of counties would account for a disproportionate share of production at risk. Fourth, irrigation was not anticipated to moderate heat damage in a setting in which water is already abundant, and part of the yield loss was anticipated to be offset by an expansion of sown area, leaving the effect on total output muted.

To examine these expectations, the analysis assembled a panel of 183 county-level land units in the Sichuan Basin for 2014–2024. It constructed growing degree days and

extreme degree days from the daily mean temperature, and then estimated two-way fixed-effects models with a full set of land-management and socio-economic controls. The result was tested against alternative thresholds, alternative exposure windows, the exclusion of the record heat years, spatial heteroskedasticity- and autocorrelation-consistent (HAC) inference, and exposure-weighted specifications. The analysis addressed four objectives. First, it located the temperature at which grain yield begins to decline and characterised the shape of the response across the full temperature range. Second, it assessed whether the results are robust to spatial dependence and to the choice of threshold and window. Third, it followed the heat signal through the land-use margin to total output and yield volatility, and examined whether irrigation moderates the damage. Fourth, it identified where heat exposure and production coincide, in order to translate the estimated response into a spatial priority for climate-adaptive land management. The resulting evidence is intended to support the targeting of adaptation measures within humid cropland systems; it identifies a biophysical constraint and its spatial incidence rather than causal policy effects. The basin's humid climate is not background but an identification condition: it breaks the collinearity between heat and water deficit that prevents attribution in dryland systems.

2. Materials and Methods

2.1. Study Area

The Sichuan Basin occupies the eastern part of Sichuan Province in southwestern China (Figure 1). Its floor lies between roughly 250 m and 700 m above sea level. The Tibetan Plateau bounds the basin to the west, the Qinling Mountains to the north, and the Yunnan–Guizhou Plateau to the south. The climate is humid subtropical, with annual precipitation of 900–1200 mm concentrated in the May–September monsoon and mean July temperatures of 26–28 °C on the basin floor. The eastern basin is one of the most heat-prone agricultural regions in China: it experienced record-breaking heat and drought in August 2022 and again in 2024, and summer heat waves associated with the western Pacific subtropical high are a recurring hazard [37,38]. Sichuan produces more than 35 million tonnes of grain a year and is the largest grain-producing province in western China [47], which makes grain the crop system of greatest consequence for food security in the region. Farming on the basin floor is dominated by a rice–rapeseed rotation, while the surrounding slopes carry maize–rapeseed or maize–wheat rotations. Because the critical growth stages of rice and maize fall in July and August, this window defines the critical growth period for grain crops [7,8]. Sichuan Province contains 183 county-level administrative units, and, because the whole province is of interest, the panel covers all of them, giving 2013 observations for 2014 to 2024. After observations with a missing outcome or control variable are dropped, the estimation sample contains 1925 county-years for 177 counties. The baseline retains the two western autonomous prefectures, Ganzi and Aba, whose agro-pastoral systems differ from the basin, and a robustness check excludes them. The irrigated share of cropland averages 54% in this sample and exceeds 80% in parts of the Chengdu Plain.

2.2. Research Framework

The analysis proceeds in four stages, as summarised in Figure 2. The first stage assembles a longitudinal county-level land panel, drawing its statistics from two groups of records: gridded county-day temperature, which measures heat exposure, and government statistics, which supply the base data for the dependent and control variables. The daily reanalysis product serves one specific purpose only, namely to place the threshold estimated from the daily mean temperature on the same footing as the thresholds measured from daily maximum temperature in the crop-yield literature.

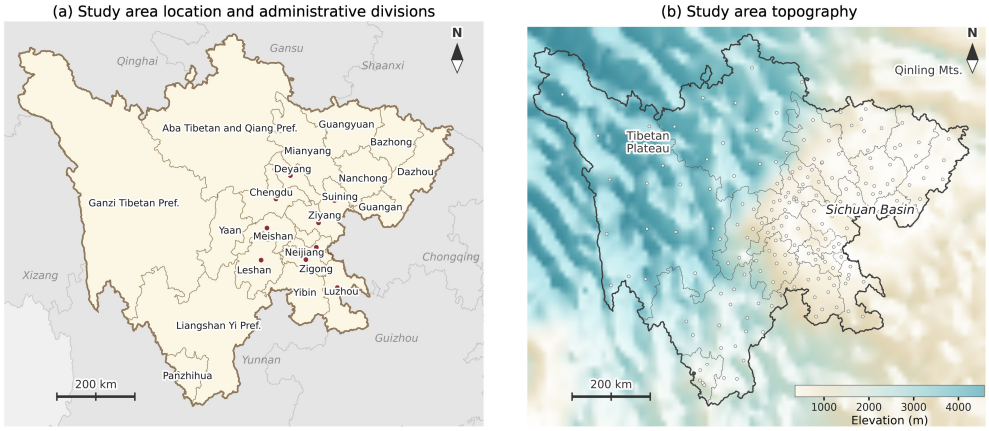


Figure 1. Study area. (**a**) Location and administrative divisions: Sichuan Province (pale yellow) with its prefecture-level divisions, each marked by a point and labelled; neighbouring provinces are labelled in grey. (**b**) Topography: Shuttle Radar Topography Mission (SRTM), 90 m relief, showing the basin floor enclosed by the Tibetan Plateau to the west, the Qinling Mountains to the north, and the Yunnan–Guizhou Plateau to the south, with the 183 county-level units shown as small points. Both panels carry a north arrow and a 200 km scale bar.

In the second stage, rather than adopting the daily mean temperature that conventional studies use as a measure of heat damage, the analysis converts the data assembled in the first stage into exposure and outcome variables. Degree days are constructed from the daily mean temperature, so that moderate warmth and extreme heat are separated by design rather than by any statistical adjustment applied later: the growing degree day term is capped at the threshold, and the extreme degree day term accumulates only the exceedance above it. The coarse indices that are conventional in agro-meteorological evaluation, namely cooling and heating degree days on an 18 °C base, the annual mean temperature, and percentile exceedance days, are constructed in parallel so that they can be used for comparison and further testing. These measures are aggregated over four windows—that is, annual, growing season, July–August, and month by month—and three further outcome variables are defined, namely sown area, total output, and yield volatility, so that the heat effect can be traced from yield to sown area and total output.

The third stage estimates the heat response. A two-way fixed-effects specification with county and year fixed effects separates the heat signal from permanent differences among land units and from shocks common to all counties in a given year, such as basin-wide heat or a policy change, while a full set of land-management and socio-economic controls absorbs the main competing explanations. The threshold is not fixed in advance: the response function is recovered non-parametrically from daily temperature bins, and the threshold is varied across 30, 32, and 34 °C, with a saturated multi-threshold specification used to show what happens when the alternatives are entered together. Spatial dependence is treated as a property to be measured rather than ignored, through Conley spatial HAC standard errors at several bandwidths and a Moran's I test on the residuals. Because extreme heat is rare, the model is also re-estimated with weights proportional to within-year exposure variation and on subsamples defined by that variation, so that a genuine change in the heat response is distinguished from the zero inflation that arises in years with almost no extreme heat.

The fourth stage translates the estimates into land-management terms. The yield effect is decomposed into a land-use component and an output component, the interaction between heat and irrigation is tested explicitly, and the counties where heat exposure and grain production coincide are identified. What the paper delivers is therefore not a single

elasticity estimate but a located constraint, an assessment of how far it survives alternative measures and inference choices, and a spatial priority for adaptation.

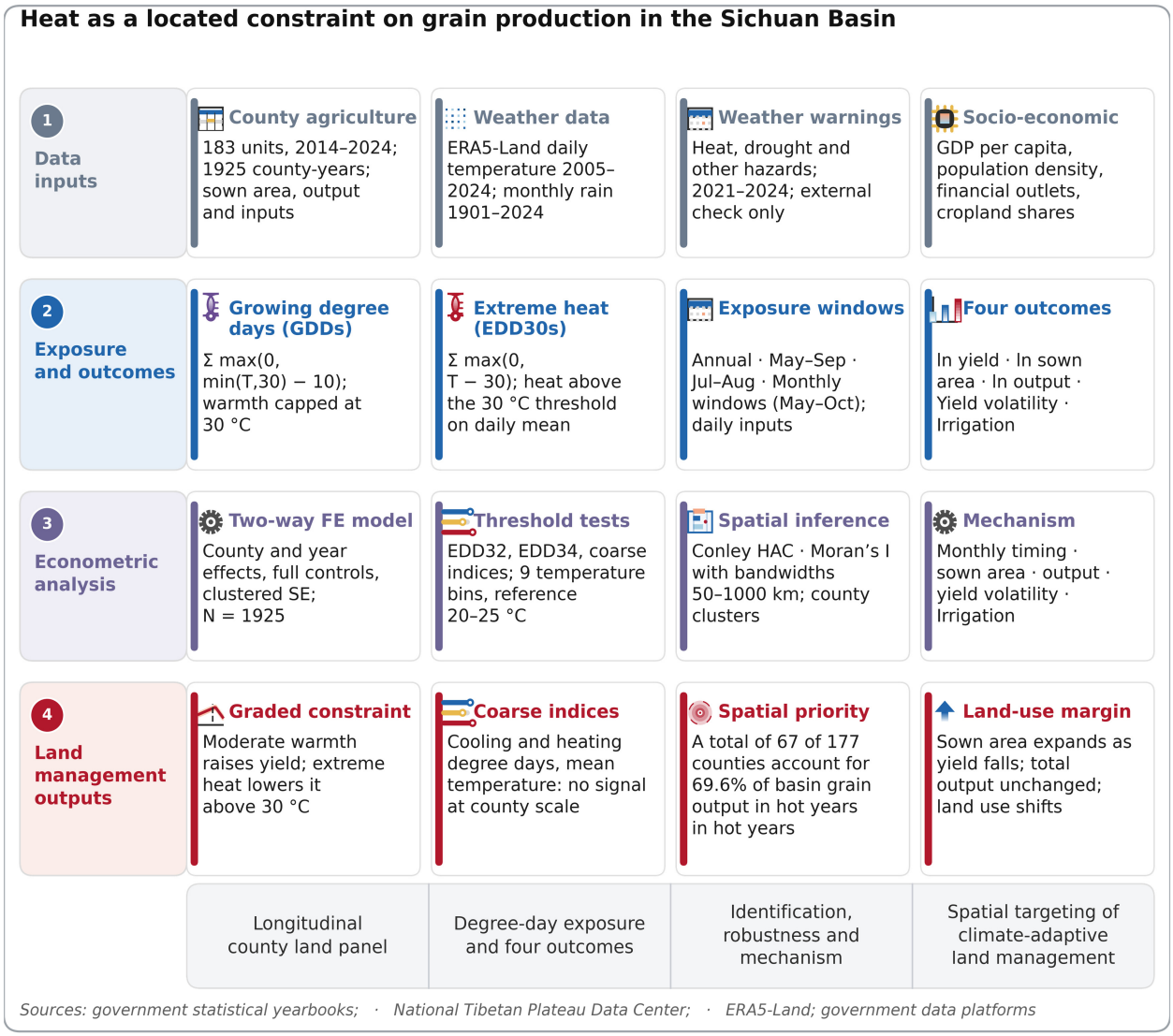


Figure 2. Research framework. Stage 1 assembles the longitudinal county land panel; Stage 2 constructs degree-day exposure, the alternative coarse measures, and the four outcomes; Stage 3 estimates the two-way fixed-effects model and tests it against alternative thresholds, windows, and spatial dependence; and Stage 4 translates the estimates into the land-use margin, the irrigation result, and a spatial priority for climate-adaptive land management.

2.3. Data

Four groups of data enter the analysis: gridded climate fields, county agricultural and land-management statistics, county socio-economic records, and administrative weather-warning records. Table 1 lists, by data type, the source, spatial resolution, and temporal coverage of each item. The ERA5-Land reanalysis supplies the daily mean surface air temperature for 2005–2024. The data have a native spatial resolution of about 0.1° and were averaged to provincial, prefecture, and county administrative boundaries (unit: °C). The years 2005–2013 serve as a fixed reference period for the percentile-based exposure measures, and the years 2014–2024 enter the estimation. Monthly precipitation comes from gridded fields published by the National Tibetan Plateau Data Center (unit: mm), and its anomaly against the 1991–2020 mean describes the water environment of the study area. In a basin where water is not the binding constraint, precipitation is held out of the

preferred specification and entered only as a robustness control. County agricultural and land-management variables come from the Sichuan Statistical Yearbook, supplemented by inquiries addressed to local government agencies. They comprise grain sown area, grain output, fertiliser consumption, rural electricity consumption, cropland area, and irrigated area. County socio-economic variables come from three sources: county statistical records, the branch registry of the National Financial Regulatory Administration, and the China Rural Financial Services Report issued by the People's Bank of China. They comprise gross domestic product (GDP) per capita, the primary-sector share, rural population, and the number of bank branches. The coordinates of each county-level unit, which correspond to the county seat for most units, come from geocoding its name with the Photon service on OpenStreetMap data, and they define the inter-county distances from which the spatial weights are built. Two further records serve purposes other than estimation. The first is the daily maximum and daily mean temperature from the ERA5-Land for 15 meteorological sites over 2015–2024, used only to place the threshold estimated here on the same footing as thresholds reported from daily maxima in the crop-yield literature. The second is county meteorological warning records for 2021–2024, used only as an external check on the spatial risk classification. Neither enters the estimation sample. Three samples appear in the paper, and their differences are mechanical rather than selective. The panel is balanced at 183 county-level units × 11 years, or 2013 county-years. The estimation sample contains 1925 county-years for 177 counties; the 88 county-years left out are concentrated in the five core urban districts of Chengdu, in Dong District, Xuzhou District, and in Hongyuan County on the western plateau, and they are excluded because grain output (46 county-years), rural population (55), or fertiliser intensity (44) are not reported for them. The volatility measure requires a three-year rolling window of output and sown area, so it is defined only from 2016 onward and covers 1572 county-years for 176 counties. The meteorological warning records are administrative and begin in 2021, and they are available for 696 of the 708 potential county-years in the estimation sample, the 12 missing records being county-years for which nothing was archived. The volatility and warning samples are used only in the mechanism and validation checks, not in the baseline estimates.

Table 1. Data types, sources, spatial resolutions, and temporal coverage.

Data Type	Variables	Source	Resolution/Coverage
Daily mean air temperature	GDD, EDD30, EDD32, EDD34, CDD18, HDD18, percentile exceedance days, mean temperature	ERA5-Land reanalysis, Copernicus Climate Data Store (https://cds.climate.copernicus.eu/datasets/reanalysis-era5-land, accessed on 1 September 2025)	0.1°; daily, 2005–2024
Daily maximum air temperature	Threshold correspondence only	ERA5-Land reanalysis, Copernicus Climate Data Store (https://cds.climate.copernicus.eu/datasets/reanalysis-era5-land, accessed on 1 September 2025)	15 meteorological sites; daily, 2015–2024
Monthly precipitation	Precipitation anomaly	National Tibetan Plateau Data Center (https://data.tpdc.ac.cn, accessed on 1 September 2025)	1 km; monthly, 1901–2024
County agricultural and land-management statistics	Grain sown area, grain output, fertiliser consumption, rural electricity consumption, cropland area, irrigated area	Sichuan Statistical Yearbook (http://tjj.sc.gov.cn/scstjj/c112132/pic_list.shtml, accessed on 1 September 2025), supplemented by inquiries to local government agencies	County-year, 2014–2024

Table 1. *Cont.*

Data Type	Variables	Source	Resolution/Coverage
County socio-economic statistics	GDP per capita, primary-sector share, rural population	County statistical records (http://tjj.sc.gov.cn/scstjj/c112132/pic_list.shtml, accessed on 1 September 2025)	County-year, 2014–2024
Financial infrastructure	Number of bank branches	National Financial Regulatory Administration branch registry (https://www.nfra.gov.cn, accessed on 1 September 2025); People's Bank of China, China Rural Financial Services Report (http://www.pbc.gov.cn, accessed on 1 September 2025)	County-year, 2014–2024
County coordinates	Inter-county distances and spatial weights	Photon geocoding service on OpenStreetMap data (https://photon.komoot.io, accessed on 1 September 2025)	183 county seats; 2024
Administrative boundaries and terrain	Study-area map and spatial weights	GADM v4.1 (https://geodata.ucdavis.edu/gadm/, accessed on 1 September 2025); SRTM 90 m elevation via CGIAR-CSI (https://srtm.csi.cgiar.org, accessed on 1 September 2025)	Vector; 90 m
Meteorological warnings	Warning counts by hazard type	National Emergency Broadcasting platform, warning information query (https://www.cneb.gov.cn/2026yjxx/, accessed on 1 September 2025)	County-year, 2021–2024

Notes: The county panel is unbalanced, and the weather-warning records cover 2021–2024 only.

2.4. Variable Construction

Following the existing literature, heat exposure for grain crops is measured by degree days [13,20]; these studies use accumulated degree days rather than mean temperature because degree days represent the heat that actually drives crop development and allow moderate warmth and extreme heat to be measured separately. Growing degree days are defined in Equation (1) and extreme degree days in Equation (2), where T_d is the daily mean temperature on day d. The growing degree day term has a lower base of 10 °C and is capped at 30 °C, whereas the extreme degree day term has a base of 30 °C and no upper bound. The two measures therefore represent, respectively, the moderate warmth that crop growth requires and the heat stress that arises once a physiological threshold is exceeded. Although both involve a value of 30 °C, their marginal contributions do not overlap, so the two are not double-counted. On any day at or above 30 °C, the growing degree day term contributes its cap of 20 degree-days and stops rising, while the extreme degree day term begins to contribute the excess above 30 °C; the two measures are consequently piecewise continuous at the threshold, so that the marginal response to temperature passes from the one to the other instead of being counted twice.

$$\mathrm{GDD} = \sum_{d} \max(0, \min(T_d, 30) - 10) \tag{1}$$

$$\mathrm{EDD30} = \sum_{d} \max(0, T_d - 30) \tag{2}$$

The choice of threshold follows the same literature. Crop-yield studies construct degree days from the daily mean temperature with high-temperature thresholds of 29, 32,

and 34 °C, above which damage is sharply nonlinear [13]; a base of 30 °C is the reference for extreme heat in that work [19], and degree-day measures of this form outperform mean temperature in explaining yields [20]. The same value appears in the agronomic literature on heat-induced spikelet sterility in rice and on kernel set in maize [7,8], and it is likewise the reference for extreme heat in the aggregate-output literature [19,28]. A base of 30 °C is therefore adopted here. Because much of the crop-yield literature measures exposure from daily maximum rather than daily mean temperature, the two definitions were related directly so that the estimates obtained here can be compared with that work. In this region, a daily mean of 30 °C corresponds to a daily maximum of about 34.5 °C, and the ERA5-Land sample gives the linear relation in Equation (3), whose intercept varies across sites from about 4.2 °C in the northeast of the basin to about 5.3 °C in the Chengdu Plain. ERA5-Land is also known to underestimate air temperature in complex terrain, with accuracy declining as altitude rises [48], and the station comparison made here puts the underestimate at the hot end of the distribution at about 3 °C. The mapping is therefore approximate and is used only for comparison with existing work, not to construct the exposure variables.

$$T_{\max} = 3.680 + 1.028 \times T_{\text{mean}};\ R^2 = 0.97,\ n = 54,795 \tag{3}$$

Alongside the preferred measure, three further groups of exposure variables serve as comparators, so that the results can be tested against the definition of exposure on which they rest. Two considerations guide the choice of degree-day exposure rather than seasonal means: crop models systematically understate the damage caused by short heat episodes [49], and degree-day measures track the yield response of grain crops to accumulated warmth in Chinese production regions [50]. Thresholds are treated as stage-specific, following agronomic work that identifies separate trigger temperatures for vegetative and reproductive stages [51]. The first group raises the threshold to extreme degree days above 32 °C (EDD32s) and above 34 °C (EDD34s), in order to examine whether damage deepens monotonically as the base rises. The second adopts the 18 °C base that is conventional in the energy and mortality literature, namely cooling degree days (CDD18s) and heating degree days (HDD18s), in order to test whether such low-base degree days carry any information about crop heat damage. A fourth group retains a compound temperature–humidity measure as an additional comparator, because heat and humidity interact over the same seasons in much of China [52]. The third group consists of percentile exceedance days, which record the days on which the daily mean temperature exceeds each county's own 90th and 95th percentiles, with the thresholds computed over the nine years 2005–2013 as a fixed reference period. That period serves only to fix the measurement scale, and it is deliberately disjoint from the estimation period so that the thresholds do not depend on the same years that enter the estimation; because these day counts enter only as comparators, the choice of reference period leaves the preferred estimates unchanged. Exposure is then aggregated over four windows: annual, growing season (May–September), July–August, and month by month. The July–August window is preferred because it coincides with the critical growth stages of the dominant rice and maize systems. Figure 3 maps the two preferred measures across the basin.

The dependent variable is the natural logarithm of grain yield per sown hectare; that is, the natural logarithm of the ratio of grain output to sown area, following the convention of the crop-yield literature [13,27]. Six controls enter the specification, covering two dimensions [53–55]. Within the land-management dimension, fertiliser intensity per sown hectare and rural electricity consumption capture input intensity and the level of agricultural modernisation, both of which condition how far a county can adjust its production technology. Within the socio-economic dimension, GDP per capita, the primary-

sector share, and rural population describe the economic structure of the county and the size of its agricultural labour force, while the number of bank branches measures access to credit and therefore the capacity of farm households to absorb the shock of a weather disaster. Table 2 reports descriptive statistics for all variables.

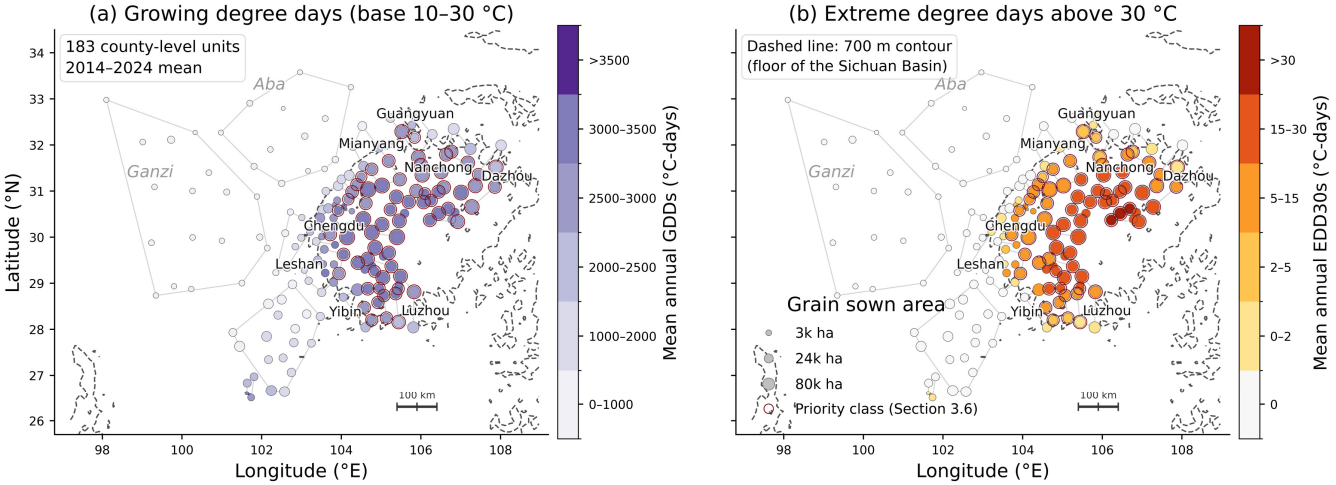


Figure 3. Spatial distribution of the two exposure measures. The two panels use deliberately different colour schemes so that the measures are not confused. (**a**) Mean annual growing degree days (GDDs, base 10 °C, capped at 30 °C) in discrete classes on a cool scale. (**b**) Mean annual extreme degree days (EDD30s, base 30 °C) in discrete classes on a warm scale, so that the 75 counties with no extreme heat at all remain visible rather than being merged into a single colour. Marker size is proportional to mean grain sown area, with a quantified size legend; open dark-red circles mark the 67 priority-class counties identified in Section 3.6; the dashed line is the 700 m contour that defines the basin floor; and a 100 km scale bar is shown in each panel. Grey polygons are convex hulls of the county coordinates within each prefecture and are indicative, not administrative boundaries.

Two further adaptation margins, heat-tolerant varieties and seed subsidies, are not included as explanatory variables. No county-level panel of varietal adoption or of cultivar heat tolerance, and no county-level breakdown of subsidy allocation, exists for the basin over 2014–2024; the same limitation applies to sowing date and to cultivar choice more generally, which are recorded in experimental or survey settings rather than annually by county. Their omission defines what the estimates describe: the heat response of the prevailing variety mix under the subsidy environment of the estimation period; that is, the damage that current land management leaves unoffset, not the damage that would remain if heat-tolerant material were widely adopted or if the design of subsidies was changed.

Table 2. Descriptive statistics for the estimation sample, 2014–2024.

Variable	Mean	SD	Min	Max	*N*
Log grain yield (t/ha)	1.608	0.272	0.574	2.258	1925
Log grain sown area (ha)	9.958	1.191	5.278	12.006	1925
Log grain output (t)	11.566	1.347	6.795	13.636	1925
GDDs, annual (°C days)	2055.5	1140.3	0.0	3776.9	1925
GDDs, May–September (°C days)	1572.5	824.2	0.0	2577.7	1925
GDDs, July–August (°C days)	747.3	376.3	0.0	1183.4	1925
EDD30s, July–August (°C days)	6.435	21.324	0.0	160.4	1925
EDD30, annual (°C days)	7.079	22.288	0.000	160.524	1925
EDD32s, annual (°C days)	0.021	0.100	0.000	0.851	1925
EDD34s, annual (°C days)	0.006	0.038	0.000	0.390	1925

Table 2. *Cont.*

Variable	Mean	SD	Min	Max	*N*
Days with daily mean ≥ 30 °C	4.3	9.2	0.0	45.0	1925
Days with daily mean ≥ 32 °C	1.3	4.5	0.0	32.0	1925
Days with daily mean ≥ 34 °C	0.4	2.4	0.0	20.0	1925
Precipitation anomaly (%)	6.274	10.455	−20.593	45.582	1925
Log GDP per capita (yuan)	10.612	0.552	8.886	12.120	1925
Log primary-sector share	−1.888	0.672	−6.481	−0.587	1925
Log rural population (10^4)	2.744	0.898	−0.916	4.420	1925
Log bank branches (count)	4.069	0.855	0.693	5.635	1925
Log rural electricity (10^4 kWh)	8.742	1.390	3.045	11.365	1925
Log fertiliser intensity (t/ha)	−1.356	1.039	−5.889	1.407	1925
Irrigated share of cropland	0.543	0.342	0.002	2.750	1925
Agricultural machinery (kW/ha)	10.079	11.752	0.342	180.897	1925
Yield volatility, 3-year CV	0.028	0.043	0.000	0.555	1572 [a]
Weather warnings issued (count)	85.948	88.705	0.000	541.000	696 [b]

Notes: GDDs and EDDs are in degree-days. Coefficients in Tables 3–6 are expressed per 100 degree-days; those in Table 7 are expressed per degree-day. The panel is balanced at 183 county-level units × 11 years (2013 county-years), of which 1925 county-years for 177 counties enter the estimates; the 88 county-years excluded are those without reported grain output, rural population, or fertiliser intensity, and they are concentrated in the urban core districts of Chengdu and in a few peripheral units. *N* therefore varies by variable: 1925 for output, exposure, and control variables, 1572 for the three-year yield CV, which requires a three-year rolling window and is defined only from 2016, and 696 for the weather-warning count, which covers 2021–2024. [a] Three-year rolling window, defined from 2016. [b] Weather-warning records, available for 2021–2024 only.

Table 3. Two-way fixed-effects estimates of the effect of moderate warmth and extreme heat on grain yield.

Specification	GDD	SE	EDD30	SE	*N*	Counties	Within R^2
(1) Annual (full year)	0.0012	(0.0021)	−0.0252 ***	(0.0071)	1925	177	0.252
(2) Growing season, May–September	0.0084 **	(0.0036)	−0.0285 ***	(0.0064)	1925	177	0.254
(3) July–August (preferred)	0.0270 ***	(0.0085)	−0.0324 ***	(0.0070)	1925	177	0.257
(4) Excluding Ganzi and Aba	0.0094	(0.0074)	−0.0294 ***	(0.0072)	1595	147	0.356
(5) Excluding 2022	0.0366 ***	(0.0109)	−0.0859 ***	(0.0275)	1750	177	0.262
(6) Excluding 2022 and 2024	0.0309 ***	(0.0107)	−0.0715 **	(0.0298)	1578	177	0.253
(7) 2017–2024 only	−0.0038	(0.0036)	−0.0115 ***	(0.0029)	1397	176	0.210
(8) Standardised (per 1 SD)	0.1015 ***	(0.0318)	−0.0069 ***	(0.0015)	1925	177	0.257
(9) SE clustered by prefecture	0.0270 *	(0.0145)	−0.0324 ***	(0.0110)	1925	177	0.257

Notes: Coefficients are expressed per 100 degree-days unless otherwise stated; row (8) reports coefficients per one standard deviation of the regressor. All coefficients are in log points and standard errors are in parentheses. Rows (1)–(8) use county-clustered standard errors and row (9) prefecture-clustered standard errors. Every specification includes county and year fixed effects and the full set of land-management and socio-economic controls. * $p < 0.10$, ** $p < 0.05$, *** $p < 0.01$.

Table 4. Alternative temperature measures and tests of threshold sensitivity.

Measure	Coef.	SE	*p*	Sig.	*N*
Panel A. Thresholds entered separately					
EDD30s (base 30 °C)	−0.0252	(0.0071)	0.000	***	1925
EDD32s (base 32 °C)	−0.0458	(0.0114)	0.000	***	1925
EDD34s (base 34 °C)	−0.1023	(0.0237)	0.000	***	1925

Table 4. *Cont.*

Measure	Coef.	SE	*p*	Sig.	*N*
Panel B. Coarse and conventional measures					
Cooling degree days (CDD18s)	−0.0030	(0.0028)	0.290		1925
Heating degree days (HDD18s)	0.0023	(0.0026)	0.385		1925
Days above county P90	−0.0002	(0.0003)	0.560		1925
Days above county P95	0.0001	(0.0003)	0.809		1925
Annual mean temperature	−0.0087	(0.0076)	0.251		1925
Panel C. Saturated specification (diagnostic only)					
EDD30s entered with EDD32s and EDD34s	−0.0513	(0.0273)	0.062	*	1925
EDD32s in the saturated model	0.1005	(0.0721)	0.165		1925
EDD34s in the saturated model	−0.1255	(0.0853)	0.143		1925

Notes: Coefficients are expressed per 100 degree-days unless otherwise stated, in log points, with county-clustered standard errors in parentheses. The dependent variable is log grain yield per sown hectare, and every specification includes county and year fixed effects and the full set of controls. Panel A compares thresholds entered one at a time; Panel B reports measures conventional in land evaluation, where the CDD18s and HDD18s are per 100 degree-days, the percentile day counts per 100 days, and mean temperature per 100 °C; Panel C enters three overlapping thresholds together and is reported as a diagnostic only. * $p < 0.10$, *** $p < 0.01$.

Table 5. Robustness of the extreme-heat coefficient to spatial dependence.

Inference/Sample	Bandwidth	Coef.	SE	t	*p*
Baseline (county-clustered)	n.a.	−0.03236	0.00702	−4.61	0.0000
Baseline (prefecture-clustered)	n.a.	−0.03236	0.01103	−2.93	0.0082
Excl. Ganzi and Aba (county-clustered)	n.a.	−0.02940	0.00720	−4.08	0.0001
Conley spatial HAC	n.a.	−0.03236	0.00699	−4.63	0.0000
Conley spatial HAC	50 km	−0.03236	0.00751	−4.31	0.0000
Conley spatial HAC	100 km	−0.03236	0.00894	−3.62	0.0004
Conley spatial HAC	200 km	−0.03236	0.01021	−3.17	0.0018
Conley spatial HAC	300 km	−0.03236	0.01063	−3.05	0.0027
Conley spatial HAC	500 km	−0.03236	0.00892	−3.63	0.0004
Conley spatial HAC	1000 km	−0.03236	0.00651	−4.97	0.0000

Notes: The coefficient for the July–August EDD30s is identical across rows because only the standard errors change; it is expressed per 100 degree-days in log points. "n.a." indicates that no bandwidth applies to that row. Every row uses the same 1925 county-years, 177 counties, 21 prefectures, county and year fixed effects, and the full set of controls. Conley standard errors use a Bartlett kernel with the bandwidth shown, and always treat observations in the same county as correlated. Moran's I on the county-year residuals is 0.200 with same-year five-nearest weights (z = 15.45) and 0.214 with 50 km distance weights.

Table 6. Temporal stability, exposure-weighted robustness, and additional specification checks.

Sample/Specification	Window	Coef.	SE	*p*	*N*
Panel A. Expanding windows					
Expanding	2014–2018	−0.09691 *	(0.04999)	0.0542	879
Expanding	2014–2019	−0.08225 **	(0.03829)	0.0331	1054
Expanding	2014–2020	−0.07207 **	(0.03215)	0.0262	1229
Expanding	2014–2021	−0.06544 **	(0.03052)	0.0334	1404
Expanding	2014–2022	−0.03292 ***	(0.00763)	0.0000	1579
Expanding	2014–2023	−0.03060 ***	(0.00673)	0.0000	1753
Expanding	2014–2024	−0.03236 ***	(0.00702)	0.0000	1925
Panel B. Rolling five-year windows and subperiod samples					
Rolling 5 y	2014–2018	−0.09691 *	(0.04999)	0.0542	879
Rolling 5 y	2015–2019	−0.07191 *	(0.03891)	0.0663	877
Rolling 5 y	2016–2020	0.07260 **	(0.03254)	0.0269	876

Table 6. *Cont.*

Sample/Specification	Window	Coef.	SE	*p*	*N*
Panel B. Rolling five-year windows and subperiod samples					
Rolling 5 y	2017–2021	0.00890	(0.01982)	0.6539	876
Rolling 5 y	2018–2022	−0.00990 ***	(0.00289)	0.0008	875
Rolling 5 y	2019–2023	−0.00760 ***	(0.00226)	0.0009	874
Rolling 5 y	2020–2024	−0.00716 ***	(0.00216)	0.0011	871
Period	Pre-2022	−0.06544 **	(0.03052)	0.0334	1404
Period	Post-2022	−0.00704 ***	(0.00195)	0.0004	521
Period	Full	−0.03236 ***	(0.00702)	0.0000	1925
Panel C. Exposure-weighted and diagnostic rows					
WLS weighted by within-year SD of EDD30s		−0.02489 ***	(0.00565)	0.0000	1925
Years with within-year SD above median		−0.03896 ***	(0.01144)	0.0008	875
Years with within-year SD above 5 degree-days		−0.03115 ***	(0.00809)	0.0002	698
Years with within-year SD above 2 degree-days		−0.02916 ***	(0.00692)	0.0000	1224
County-years with EDD30s > 0 only		−0.02813 ***	(0.01037)	0.0078	682
Baseline (all county-years)		−0.03236 ***	(0.00702)	0.0000	1925
[diagnostic] 2016–2020 window, all		0.07260 **	(0.03254)	0.0269	876
[diagnostic] 2016–2020, EDD30s > 0 only		0.02834	(0.03468)	0.4162	283
Panel D. Additional specification checks (precipitation control)					
EDD30s with precipitation control		−0.03409 ***	(0.00697)	0.0000	1925
GDDs with precipitation control		0.02025 **	(0.00916)	0.0284	1925
Precipitation anomaly		−0.00058	(0.00040)	0.1435	1925

Notes: Coefficients are expressed per 100 degree-days unless otherwise stated, in log points, with county-clustered standard errors in parentheses; all rows include county and year fixed effects and the full set of controls, and the dependent variable is log grain yield per sown hectare. Panels A and B vary the sample window, Panel C reweights or restricts the sample to address the zero inflation that arises because extreme heat is rare, and Panel D adds the annual precipitation anomaly to the preferred specification. * $p < 0.10$, ** $p < 0.05$, *** $p < 0.01$.

Table 7. Mechanisms: phenological timing, land use, and the moderating role of irrigation.

Specification	Term	Coef.	SE	*p*
Monthly (separate)	EDD30s in May	−0.014249	(0.012774)	0.266
Monthly (separate)	EDD30s in June	−0.001390	(0.002799)	0.620
Monthly (separate)	EDD30s in July	−0.002036 ***	(0.000466)	0.000
Monthly (separate)	EDD30s in August	−0.000348 ***	(0.000077)	0.000
Monthly (separate)	EDD30s in September	−0.000223	(0.000224)	0.321
Monthly (joint)	July, entered jointly	−0.002072 ***	(0.000705)	0.004
Monthly (joint)	August, entered jointly	−0.000007	(0.000104)	0.944
Land use	Log sown area	0.000218 **	(0.000097)	0.025
Output	Log total output	−0.000106	(0.000097)	0.275
Volatility	Yield volatility (3-year CV)	0.000142 ***	(0.000029)	0.000
Irrigation	EDD30s × high-irrigation county	0.004362	(0.006764)	0.520
Heat history	EDD30s × historically hot county	0.234170	(0.175490)	0.184
Event split	EDD30s in record years (2022, 2024)	−0.033022 ***	(0.007169)	0.000
Event split	EDD30s in other years	−0.067589 ***	(0.025843)	0.010

Notes: The first ten rows are expressed per degree-day, because month-specific exposure has small support (the July EDD30s average only about 2.5 degree-days); multiply by 100 to read them per 100 degree-days. The last four rows are expressed per 100 degree-days. The first five rows enter each month on its own and the next two enter July and August together; the land-use, output, and volatility rows replace the dependent variable as indicated and are read from the same preferred specification. The two event-split rows report the EDD30 slope separately for the two record years and for all other years; the two slopes are not statistically different ($p = 0.130$). Every row includes county and year fixed effects, the full set of controls, and county-clustered standard errors. ** $p < 0.05$, *** $p < 0.01$.

2.5. Empirical Strategy

To isolate the heat signal from permanent differences among land units and from shocks common to all counties in a year, estimation is based on a two-way fixed-effects model:

$$\text{lnyield}_{it} = \beta_1 \text{GDD}_{it} + \beta_2 \text{EDD30}_{it} + \gamma' X_{it} + \mu_i + \lambda_t + \varepsilon_{it} \quad (4)$$

In Equation (4), i indexes counties and t years; μ_i and λ_t are county and year fixed effects; X_{it} is the vector of controls; and ε_{it} is the error term. GDDs and EDD30s enter jointly so that the level of warmth and the incidence of extreme heat are separately identified. Because the dependent variable is in logarithms and exposure is in degree-days, each coefficient is read as a proportional change in yield per degree-day, and the tables report the same coefficients per 100 degree-days. All estimations were performed in Stata 18 (StataCorp LLC, College Station, TX, USA), with standard errors clustered at the county level. Three features of the implementation deserve to be stated explicitly. First, the model is estimated by the within transformation for counties together with year indicators, so that each coefficient is identified from deviations of a county from its own mean and of a year from the basin-wide mean; a small number of county-years drop out because the outcome or a control is not reported, and the estimate therefore uses every county-year for which the full set of variables is observed. Second, the identifying assumption is that, conditional on the fixed effects and the controls, within-county fluctuations in temperature are uncorrelated with other determinants of yield. The specification therefore does not require counties to be comparable with one another, only that a county's deviations from its own average are not systematically related to omitted factors. Third, standard errors are clustered at the county level throughout, which permits arbitrary correlation within a county over time, and the spatial-inference checks described in Section 2.6 relax the assumption that correlation stops at the county boundary. Coefficients are reported per 100 degree-days in Tables 3–6 and 8. Table 7 reports the month-specific and decomposition rows per degree-day, because monthly exposure has small support, and its four dummy-based rows per 100 degree-days, as its note states.

Identification rests on within-county and within-year variation, which is the source of variation that climate-econometric studies rely on when permanent differences among locations must be separated from weather shocks [30,56]. EDD30s have substantially more within-county than between-county variation, with a within-county standard deviation of 20.2 degree-days against a between-county standard deviation of 9.4, which is what a fixed-effects design requires. The opposite holds for GDDs (within 79, between 820 degree-days). Once the county fixed effects absorb that cross-sectional spread, the moderate-warmth coefficient is identified from a comparatively narrow band of within-county variation. It therefore rests on less identifying variation than the extreme-heat coefficient, and is correspondingly less precisely estimated [30,36,57]. This asymmetry is a property of the design rather than a defect of the data, and it explains why the moderate-warmth coefficient loses significance in several of the robustness specifications while the extreme-heat coefficient does not.

2.6. Robustness Strategy

The estimates are exposed to three threats, and seven checks were specified in advance to address them. The first threat is that the result is carried by particular counties or particular years. The second is that inference is too optimistic because heat exposure is spatially clustered. The third is that the estimated response depends on how exposure is measured.

Table 8. The heat effect under alternative water-availability, irrigation, and terrain specifications.

Specification	EDD30	Additional Term	*N*
Preferred specification (Table 3)	−3.24% ***	—	1925
+ Arable land area	−3.26% ***	Ln cropland area: 0.002% (p = 0.895)	1925
+ Terrain interaction	−5.68% ***	× Relief (standardised): −0.027% (p = 0.160)	1925
+ Dry-year interaction	Wet −1.86% ***; dry −4.38% ***	× Dry year: −2.52% ***	1925
+ Irrigation, and its interaction with a dry year	−1.83% **	× Irrigation: 1.48% (p = 0.242); × irrigation × dry: −1.08% (p = 0.385)	1925
+ Core-period precipitation anomaly	−3.77% ***	× Anomaly: 0.016% (p = 0.498)	1925
+ SPI-3 ending in August	−3.01% ***	× SPI-3: 0.003% (p = 0.676)	1925
+ Soil moisture	−3.05% *	× Soil moisture: −0.0001% (p = 0.908)	1925
Dry county-years only	−2.41% (p = 0.110)	—	469
Wet county-years only	−1.44% *	—	1456
+ Large and medium reservoir count	−3.27% ***	× Reservoirs (standardised): 0.05% (p = 0.864)	1925
+ Large and medium reservoirs per unit cropland	−3.01% ***	× Reservoirs per 10,000 ha: −0.58% (p = 0.568)	1925
Counties with vs without a large or medium reservoir	With −2.19% *** (N = 975); without −4.37% *** (N = 950)	—	1925
Daily maximum, 35 °C base (ERA5-Land, all 183 counties)	EDD35s −2.06% ***	GDDs on daily maximum: 1.72% *	1925
Same source, 34 °C base	EDD34s −1.75% ***	GDDs on daily maximum: 1.80% *	1925
Same source, daily mean for comparison	EDD30s −1.96% ***	GDDs on daily mean: 2.43% **	1925
Daily maximum, 35 °C base (MERRA-2, all 183 counties)	EDD35s −1.97% **	GDDs on daily maximum: 2.27% ***	1925
Same source, daily mean for comparison	EDD30s −3.31% **	GDDs on daily mean: 4.00% ***	1925

Notes: A leading "+" marks the rows that extend the preferred specification of Table 3 by the term named in the first column; the third column reports the coefficient on that term or on the interaction it defines, and in the daily maximum rows, where the exposure measure itself is replaced, it reports the companion GDD coefficient. The dependent variable, the six controls, county and year fixed effects, and county-clustered standard errors are unchanged. EDD30s are expressed per 100 degree-days, and standard errors are clustered by county. Dry county-years are those whose core-period precipitation anomaly falls below the sample 25th percentile. Irrigation does not moderate the heat effect on its own or interact with the dry-year indicator, so the null in Table 7 survives the test of whether irrigation matters where water supply is most likely to bind. In the daily maximum rows, the exposure is built from the daily maximum temperature with the threshold raised to its daily maximum equivalent; because the two exposures are scaled differently, the 100 degree-days value is not the same physical quantity across rows, and the comparable statement is per standard deviation: the daily maximum and daily mean measures imply −0.27% and −0.29% per standard deviation in the MERRA-2 sample, and −0.53% and −0.47% in the ERA5-Land sample. Reservoir counts are taken from the annual lists of large and medium reservoirs published by the Sichuan Provincial Department of Water Resources and by the Ministry of Water Resources; those lists are complete for the two size classes, so a county absent from them is recorded as having none. Cumulative storage capacity is reported for only 34 of the 183 counties and is therefore not used in the regressions. "×" denotes an interaction of that term with EDD30s and "—" that no additional term is defined for that row. * $p < 0.10$, ** $p < 0.05$, *** $p < 0.01$.

To address the first threat, the Ganzi and Aba autonomous prefectures were excluded, because their agro-pastoral systems differ from the basin, and then 2022 and 2024, the record heat years. A further check re-estimated the model on 2017–2024, because the sown-area figures for 2014 and the rural-economy variables for 2016 are affected by a mis-labelled yearbook table.

To address the second threat, Conley spatial HAC standard errors were reported at bandwidths from 50 km to 1000 km [34], following the implementation described for arbitrary correlation structures [58]. Conley standard errors allow correlation to decay with geographic distance rather than stopping at the county boundary, so they test whether the county-clustered inference survives the spatial structure that the residuals in fact exhibit. Spatial dependence was also tested directly, using Moran's I computed on the county-year residuals with two sets of spatial weights: inverse-distance weights over counties lying within a given bandwidth, and k-nearest-neighbour weights [59–61]. The test is applied to county-year rather than county-mean residuals because the fixed effects force the within-county mean of the residuals to zero, which would leave a Moran's I computed on county means numerically empty.

To address the third threat, the EDD30s were replaced with EDD32s, EDD34s, CDD18s, HDD18s, the annual mean temperature, and percentile-based day counts, so that the measures actually used in land suitability and land capability mapping were tested rather than assumed adequate [32,33]. Two further specifications addressed the distribution of the preferred regressor: the model was re-estimated with weights proportional to the within-year standard deviation of EDD30s, and on subsamples defined by that standard deviation. Because extreme heat is absent from many county-years, unweighted estimates in those years largely compare zeros with zeros, and these specifications separate a genuine change in the heat response from that zero inflation. A final check added the annual precipitation anomaly to the preferred specification, so that the heat coefficient can be shown not to be a proxy for water deficit. To make the mapping between threats and checks explicit, the seven pre-specified checks are as follows: (i) exclusion of the two autonomous prefectures; (ii) exclusion of the record years; (iii) re-estimation on 2017–2024; (iv) Conley spatial HAC inference at bandwidths from 50 km to 1000 km, alongside county- and prefecture-clustered standard errors; (v) Moran's I computed on the county-year residuals with distance-band and k-nearest-neighbour weights; (vi) replacement of the EDD30s by EDD32s, EDD34s, CDD18s, HDD18s, the annual mean temperature, and percentile-based day counts, together with the exposure-weighted and variance-restricted specifications that separate a genuine change in the heat response from zero inflation; and (vii) addition of the precipitation anomaly. Four checks added at revision extend the same logic and are reported in Table 8: degree days constructed from the daily maximum rather than the daily mean temperature; arable-land area and terrain ruggedness as additional controls and as interactions; interactions of EDD30s with irrigation, with three independent indicators of water availability (the core-period precipitation anomaly, the three-month standardised precipitation index ending in August, and soil moisture) and with a dry-year indicator; and a triple interaction of EDD30s with irrigation and the dry-year indicator, which tests whether irrigation matters precisely where water supply is most likely to bind.

3. Results

3.1. The Temperature–Yield Relationship Is Nonlinear and Window-Specific

Table 3 reports the estimates for the annual, growing-season, and July–August exposure windows. The question addressed here is which window, and which part of the temperature distribution, carries the constraint on grain yield. Moderate warmth is a resource that the crop requires in order to complete development, whereas heat above

30 °C is a stressor, and the two differ not only in sign but in the way they vary. Over the full year, the effect of growing degree days on grain yield is not significant, and the effect of extreme degree days, although significantly negative, is markedly smaller in absolute value, so that the annual window dilutes the beneficial and damaging parts of the signal at the same time. Over the growing season, the positive effect of growing degree days and the negative effect of extreme degree days both become significant, but their absolute magnitudes remain smaller than in the July–August window. In that window, the contrast is sharpest: an additional 100 growing degree days raises the grain yield by 2.70% and an additional 100 extreme degree days lowers it by 3.24%, both significant beyond the 1% level. July–August is therefore the window in which the heat constraint actually binds, and a wider window averages a phenologically concentrated signal into insignificance.

The robustness specifications point the same way. Excluding the two autonomous prefectures of Ganzi and Aba removes the significance of the positive growing degree day effect, while the negative extreme degree day effect remains significant at the 1% level, so the damage does not depend on the western highland sample. Excluding 2022, or both 2022 and 2024, enlarges the absolute value of the extreme-heat coefficient, which shows that the estimate does not depend on the record years and that damage in extreme years may be amplified nonlinearly. In the 2017–2024 subsample, the positive growing degree day effect loses significance while the extreme-heat effect remains highly significant, which shows that the moderate-warmth term rests on less identifying variation and is estimated less precisely. In the standardised specification, a one-standard-deviation increase in growing degree days raises the yield by 10.2% and a one-standard-deviation increase in extreme degree days lowers it by 0.69%, both in log points. The comparison should not be read as a ranking of marginal effects: the standard deviation of the July–August GDDs is 376.3 degree-days whereas that of EDD30s is 21.3, so a one-standard-deviation change in GDDs represents far more accumulated heat than the equivalent change in EDD30s, and the larger standardised coefficient of GDDs reflects the spread of the regressor rather than a stronger marginal influence. What it does establish is that the extreme-heat term, small on average, varies sharply from year to year and therefore carries most of the climate risk. With prefecture-level clustering, the extreme-heat coefficient remains significant at the 1% level, so the result survives a stricter spatial clustering of the standard errors. Taken together, the negative effect of extreme heat is robust in every specification whereas the positive effect of moderate warmth is comparatively fragile, which confirms the reality and the importance of the heat constraint in the July–August window.

Figure 4 reports the same relationship non-parametrically, so that the parametric estimates of Table 3 and the bin-by-bin profile of Figure 4 serve as mutual checks: the bins impose no functional form, whereas the parametric model delivers the coefficients used throughout the paper. The two cannot be compared numerically, because the bins are per day and the coefficients are per 100 degree-days, but they agree in sign and in the temperature at which damage begins. The figure takes the window identified in Table 3 as given and places daily mean temperature bins on the horizontal axis and the coefficient of each bin relative to the 20–25 °C reference bin on the vertical axis, from a two-way fixed-effects model with the full set of controls. Damage to grain yield in the basin does not appear suddenly at a single critical value, but deepens step by step as temperature rises. The 20–25 °C bin is the reference interval and its coefficient is normalised to zero, with every other bin reported against it. Below the reference interval, the coefficients are small and mostly insignificant, so crop yield is not sensitive to temperature in that range. Above it, the 25–30 °C bins are already negative but limited in magnitude, so that damage is not yet established. From 30 °C, the coefficients begin to fall clearly, and above 34 °C, they turn sharply negative, at which point damage becomes pronounced: an additional

day above 34 °C lowers the grain yield by about 0.35%, roughly 4.5 times the cost of a day in the 30–32 °C bin. Because the response is monotone in temperature above the reference bin, a shape of this kind is better read as a graded biophysical constraint than as a statistical artefact of the chosen threshold [13,21]. The nonlinearity also has a practical implication for land evaluation: a single degree-day coefficient computed over the whole summer understates the damage incurred in the hottest years.

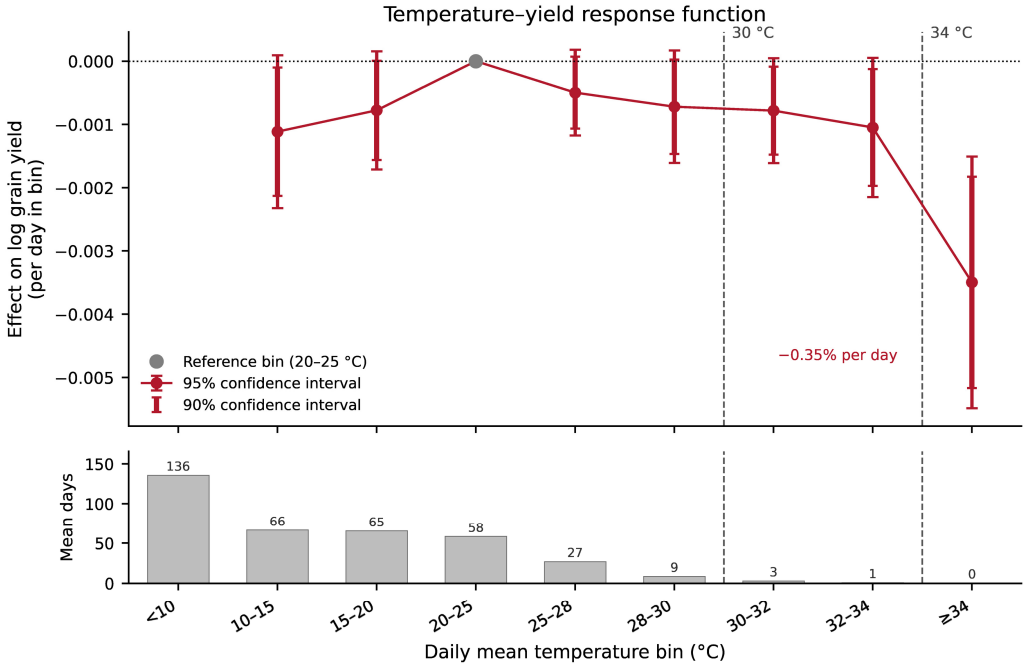


Figure 4. Temperature–yield response function. The (**upper**) panel gives the coefficient on the number of days falling in each daily mean temperature bin, relative to the 20–25 °C reference bin (grey point), from a two-way fixed-effects model with the full set of controls; dark and light whiskers are 95% and 90% confidence intervals based on county-clustered standard errors. The (**lower**) panel gives the mean number of days per year in each bin for the estimation sample, so that the support behind each coefficient is visible. Dashed vertical lines mark the 30 °C base of EDD30s and the 34 °C point above which damage accelerates. Bin coefficients are per day and are not numerically comparable with the per-100-degree-day coefficients in Tables 3 and 4, although the two agree in sign and in the temperature at which damage begins.

Turning to the time dimension, Figure 5 reports the month-specific effect of extreme degree days on grain yield, with months on the horizontal axis and the coefficient of each month's EDD30s on the vertical axis, for two sets of estimates: each month entered on its own, and the summer months entered jointly. Magnitude and precision must be read separately here: the May coefficient is large but so imprecisely estimated that it cannot be distinguished from zero, whereas the summer coefficients are small and precisely estimated, and July carries by far the largest of them. Damage is thus strongly concentrated in time. When the months are entered separately, July and August are each significantly negative, but the July coefficient (−0.00204) is about six times the August coefficient (−0.00035), and May, June, and September cannot be distinguished from zero. When July and August enter jointly, the July coefficient retains its full magnitude while the August coefficient collapses to zero. The divergence between two adjacent months matters because it reveals a mismatch between exposure and damage: most extreme degree days occur in August, whereas the marginal damage is carried by July, which corresponds to heading and early grain filling in basin rice and to tasselling in maize [25]. It follows that the damage is more likely to arise from a direct effect on the crop itself than from water shortage. The timing evidence

therefore points to a direct physiological mechanism operating at a specific phenological stage rather than to a water-deficit channel spread across the growing season [11].

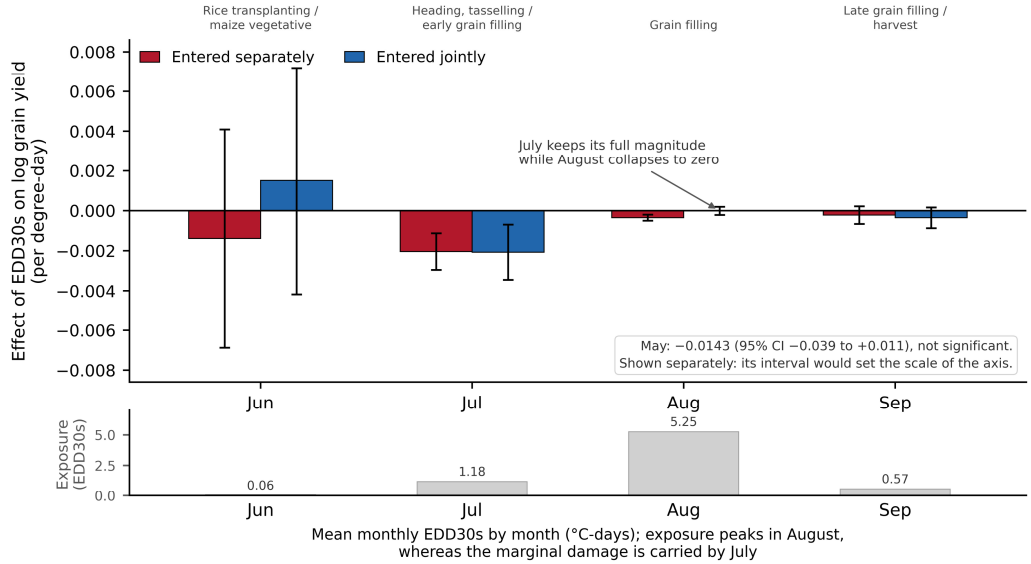


Figure 5. Month-specific effects of extreme degree days on grain yield, June to September. In the (**upper**) panel, red bars enter each month on its own and blue bars enter the four summer months jointly; whiskers are 95% confidence intervals based on county-clustered standard errors. The (**lower**) panel gives mean monthly exposure (EDD30s), which shows that exposure peaks in August while the marginal damage is carried by July. Phenological stages are labelled above the months. The May coefficient of −0.0143 (95% confidence interval: −0.039 to +0.011) is not plotted because it is not statistically distinguishable from zero and its interval would set the scale of the whole axis; it is reported in the text box instead.

3.2. Threshold Sensitivity and the Failure of Coarse Measures

This section asks where the threshold lies and whether the coarse climatic indices used in land evaluation detect it. Table 4 shows that the estimated damage deepens as the threshold is raised: exposure defined above 30 °C lowers the yield by about 2.52% per 100 degree-days, exposure defined above 32 °C by about 4.58%, and exposure defined above 34 °C by about 10.23%, all significant at the 1% level. These are three separate definitions of the regressor rather than three points on one response curve, so the comparison shows how far estimated severity depends on where the threshold is placed. Therefore, the effect of heat on yield does not appear suddenly at a single critical value but is a graded constraint that deepens step by step as temperature rises, so that any heat threshold carried into land evaluation embeds a judgement about severity. When the three thresholds enter the model together, the coefficients become unstable and implausible, because the three are nested and highly overlapping and compete for the same variation, which conversely shows that one well-chosen threshold is preferable to a saturated specification.

Comparison with the measures actually used in land evaluation is equally clear. Cooling and heating degree days on an 18 °C base, the annual mean temperature, and day counts above each county's own 90th and 95th percentiles are all indistinguishable from zero, and none reach even the 10% level. The reason is structural rather than incidental: an 18 °C base lies far below the range in which crop heat damage occurs, and therefore mainly captures the general warmth of the year, making it nearly collinear with growing degree days, while percentile thresholds are normalised to the local climate by construction and carry almost no information about absolute heat stress. The indices most commonly carried into land suitability and land capability mapping are therefore poorly suited to detect the heat constraint identified here. It should be noted that the statistical support for EDD32s

and EDD34s is thin, and their estimates are driven mainly by the two record years, so they should not be read as cross-year threshold effects; EDD30s, by contrast, are non-zero in every year of the sample and in a substantial minority of counties, which is why they are adopted as the headline measure.

3.3. Robustness to Spatial Dependence

The question here is whether the estimated coefficient survives inference that allows for spatial dependence. Table 5 shows that the EDD30 coefficient is −0.0324 under every inference method and that only the standard error and the level of significance change. With county clustering, the standard error is 0.00702 and the coefficient is significant at the 1% level. Because exposure is assigned at the prefecture level, the level of clustering should correspond to it, and prefecture-level clustering, which allows arbitrary correlation among the counties of a prefecture, is therefore also used [35,36]; the standard error rises to 0.01103 but the estimate remains significant at the 1% level. Excluding the two autonomous prefectures of Ganzi and Aba gives a coefficient of −0.0294 with a standard error of 0.00720, so the result is equally robust there. To accommodate correlation that decays with geographic distance, Conley spatial HAC standard errors are also used, which allow correlation to decay with distance while always treating observations in the same county as correlated [34]; they are, at most, about half again as large as the county-clustered standard errors and narrow again at the widest bandwidths—the coefficient remains significant at the 1% level at every bandwidth from 50 to 1000 km. Spatial dependence therefore raises the standard error without overturning the inference.

The residuals do show clear spatial correlation at short range. Moran's I is 0.21 at a 50 km bandwidth and decays to essentially zero by 300 km, and nearest-neighbour weights give the same picture. The dependence is therefore a local phenomenon rather than a basin-wide gradient, and it matches the residual covariance structure: county pairs within the same prefecture account for a far larger share of residual variance than pairs in different prefectures. This spatial structure is precisely what the Conley HAC standard errors in Table 5 are designed to accommodate, and they do so at every bandwidth without overturning the inference. Although spatial correlation is real, it is quantified here rather than assumed away, and the estimated heat effect survives it. The conclusion is not confined to this basin: whenever heat exposure is spatially clustered, the residuals of county-level land-productivity models will be spatially correlated, and county-clustered standard errors alone will understate the uncertainty of such estimates.

3.4. Temporal Stability and Additional Specification Checks

Table 6 tests whether the heat effect is driven by exceptional years and addresses the zero inflation that arises because extreme heat is rare. Expanding windows show a coefficient that is negative and significant at every horizon; the earliest window, 2014–2018, is larger in magnitude and much less precise, and as years are added the estimate converges towards the baseline, so additional data improve precision rather than changing the conclusion. Subperiod samples support the same reading, with both the pre-2022 and the post-2022 coefficients negative and significant. Among the rolling five-year windows, 2016–2020 yields a positive coefficient that is significant at the 5% level ($p = 0.027$), whereas every window containing 2022 is negative and highly significant; because the within-year standard deviation of extreme degree days in that window is an order of magnitude smaller than in 2022, and most county-years record no extreme heat at all, the anomaly is more likely to arise from zero inflation than from an institutional change regarding the effect of heat. Across all specifications reported in Tables 3 and 6, the estimated coefficient keeps its sign and significance, but its magnitude ranges from −9.69% per 100 degree-days in the

earliest expanding window to −1.15% in the 2017–2024 subsample, with the full-sample estimate at −3.24%; the width of this range is a property of the design, since extreme heat is absent from most county-years and the identifying variation is therefore concentrated in a small number of hot years.

To distinguish a genuine change in the heat response from zero inflation, Table 6 turns to exposure weighting and subsample specifications. Re-estimated with weights proportional to the within-year standard deviation of EDD30s, the coefficient is negative and highly significant; restricting the sample to years whose within-year standard deviation is above the median, five degree-days, or two degree-days likewise yields a negative and highly significant coefficient; finally, keeping only county-years with EDD30s above zero leaves the coefficient negative and highly significant. In particular, the positive coefficient of the 2016–2020 window becomes insignificant once county-years with zero EDD30s are excluded, which shows that the anomaly is an artefact of zero inflation rather than evidence that heat ceased to matter in the mid-2010s. Additional specification checks show that the heat coefficient is not a proxy for water deficit: when the annual precipitation anomaly is added to the preferred specification, the EDD30 coefficient keeps its sign and becomes slightly larger in absolute value, while the precipitation anomaly coefficient is indistinguishable from zero.

3.5. Mechanisms: Phenological Timing, Land Use, and Irrigation

To identify the mechanism through which the heat constraint operates, three dimensions are examined, namely phenological timing, land use, and irrigation, with the results reported in Table 7. The monthly results place the damage firmly in July. When the months are entered separately, July and August are each significantly negative, but the July coefficient is about six times the August coefficient and no other month can be distinguished from zero; when July and August enter jointly, the July coefficient retains its full magnitude while the August coefficient collapses to zero. This divergence shows a mismatch between exposure and damage: most extreme degree days occur in August, whereas the marginal damage is carried by July, which corresponds to heading and early grain filling in basin rice and to tasselling in maize and is therefore the phenological stage most sensitive to heat. The timing evidence is therefore more consistent with a direct physiological mechanism operating at a specific phenological stage than with a water-deficit channel spread across the growing season, although the two channels cannot be separated directly with these data.

Second, the results in Table 7 show that the heat signal can be traced along the land-use margin to total output and yield volatility. With log sown area as the dependent variable, the EDD30 coefficient is significantly positive, so heat modestly but significantly expands grain sown area. Because log yield equals log output minus log area, the negative yield effect decomposes into a small negative output component and a positive area component that almost cancels it, so that the result with log total output as the dependent variable is statistically indistinguishable from zero. The area response is statistically identifiable but economically small: a coefficient of 0.000218 log points per degree-day implies that 100 extreme degree days expand the sown area by about 0.02%, so the offset to the yield loss is modest rather than evidence of large-scale adaptation. Farmers therefore appear to compensate partially for lower yields by expanding cultivated area, and this land-use feedback materially changes the food-security reading of the yield result [10]. At the same time, with the three-year coefficient of variation in yield as the dependent variable, the EDD30 coefficient is significantly positive, so extreme heat raises yield volatility while lowering the mean; a constraint that depresses the mean and raises the variance costs farm households more than its average effect alone suggests.

Third, Table 7 tests whether irrigation mitigates heat damage. The interaction between EDD30s and the high-irrigation county dummy is small and insignificant, and the implied slopes in high-irrigation and low-irrigation counties are each precisely estimated and statistically indistinguishable from one another, which shows that the absence of moderation is not a matter of insufficient power in one group but a genuine null. Irrigation, the default land-management response to climatic stress in this region, does not protect grain yield against extreme heat [62]. In addition, the interaction between EDD30s and the historically hot county dummy is insignificant, so past exposure to heat does not change the marginal damage. When the EDD30 slope is allowed to differ between the two record years and all other years, it is −3.30% per 100 degree-days in 2022 and 2024 against −6.76% elsewhere; the difference is not statistically significant ($p = 0.130$). The marginal damage per degree-day therefore does not rise in the record years, and what makes those years exceptional is the level of exposure rather than the slope of the response. It should be emphasised that this evidence on mechanism is indirect: the monthly profile identifies when the constraint binds, not why it binds. July could be damaging because heat more often exceeds the threshold then, because the crop is more sensitive at that stage, or because other stressors coincide with it, and the present data cannot separate these channels. The irrigation null is consistent with a direct thermal channel, but it does not rule out the possibility that the reliability of water delivery during a heat wave, rather than the extent of irrigated area, is what matters. Alternatives such as radiation stress, or pest and disease pressure in the same weeks, cannot be excluded either, and direct testing would require field-level or station-level observations.

Because the irrigation variable measures the extent of irrigation rather than the reliability of supply, four further checks were added at revision, and they are collected in Table 8. Arable-land area enters as an additional control; terrain ruggedness enters as an interaction; EDD30s are interacted in turn with the core-period precipitation anomaly, with the three-month standardised precipitation index ending in August, and with soil moisture; and a dry-year indicator is introduced on its own, in interaction with EDD30s, and in a triple interaction with EDD30s and irrigation. Because county-level measures of irrigation reliability do not exist in the Chinese statistical system, we also assembled one from the primary public records: the annual lists of large and medium reservoirs published by the provincial water authority and by the Ministry of Water Resources, which enumerate those two size classes completely. The count of large and medium reservoirs in a county, and that count per unit cropland, enter as interactions with EDD30s. The heat coefficient is unchanged by any of these additions, ranging from −3.0% to −5.7% per 100 degree-days and remaining significant at the 1% level in all but one specification. The interaction terms themselves are indistinguishable from zero, with one exception: damage is larger in the driest county-years. That amplification is driven entirely by the two record years, since the interaction becomes positive and insignificant once 2022 and 2024 are excluded (Table 8 and Section 3.4), and it is consistent with the two stressors compounding in those years rather than with irrigation or soil moisture conditioning the response. Crucially, the interaction between EDD30s and irrigation remains insignificant both on its own and interacted with the dry-year indicator, so the irrigation null of Table 7 holds precisely where water supply is most likely to bind. Finally, the exposure itself was rebuilt from the daily maximum rather than daily mean temperature, using two independent reanalyses, because the daily mean temperature is only an approximation of physiologically relevant exposure. With the threshold raised to its daily maximum equivalent, the extreme-heat coefficient remains negative and significant in both sources (−2.06% per 100 degree-days on ERA5-Land and −1.97% on MERRA-2, each covering the full 183-county sample); within each source, the corresponding daily mean measure gives −1.96% and −3.31%, and because the two expo-

sures are scaled differently, the comparable statement is per standard deviation, where the two definitions differ by less than 0.1 percentage points.

3.6. Where Heat Exposure and Production Coincide

In Figure 6, the estimation counties are classified into four groups by whether their mean July–August extreme degree days and their mean grain output lie above or below the sample median: 68 counties are low-heat and low-output, 21 are low-heat and high-output, 21 are high-heat and low-output, and 67 are placed in the priority class because they combine above-median heat exposure with above-median output. Thus, heat exposure and grain production are not independent of one another but clearly concentrate in the same counties, and that concentration is not a scatter of isolated hotspots but a pattern with a well-defined spatial extent.

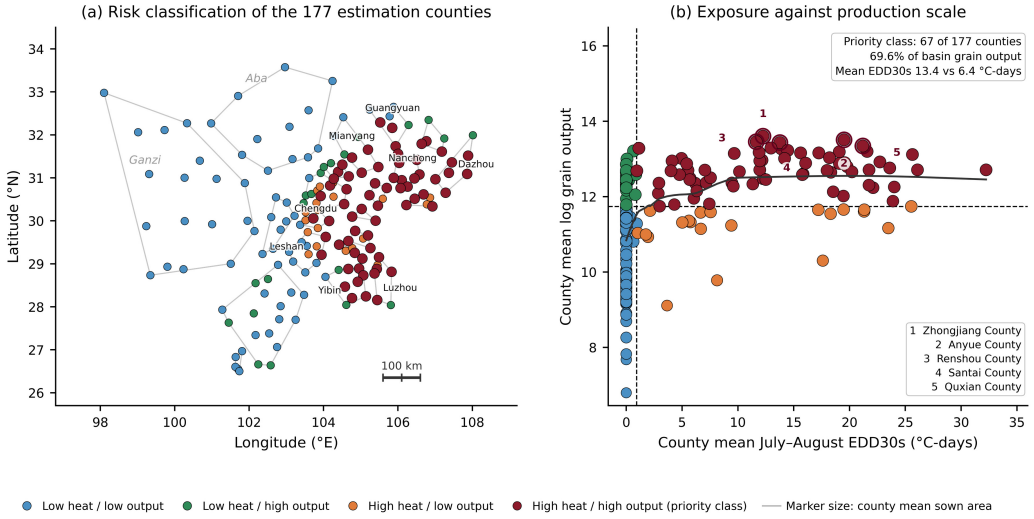


Figure 6. Spatial overlap of heat exposure and production scale, and the resulting risk classification. (**a**) The 177 estimation counties classified by whether their mean July–August EDD30s and log grain output lie above or below the sample median; major prefectures are labelled, a 100 km scale bar is shown, and grey outlines are convex hulls of the county coordinates within prefectures. (**b**) County mean EDD30s against county mean log grain output, with median lines, a locally weighted regression (LOWESS) curve through all counties, marker size proportional to mean sown area, and the five largest grain producers in the priority class circled, numbered, and named. dashed lines mark the sample medians. The panel states the number of priority counties, their share of basin grain output, and their mean exposure.

Those 67 counties together account for 69.6% of total grain output in the sample, and their mean exposure is more than twice the sample average. Spatially, they form a contiguous block in the eastern basin, spanning Nanchong, Dazhou, Guang'an, Suining, and Ziyang, and the eastern parts of Chengdu and Mianyang. Close to two-thirds of the basin's grain output therefore comes from precisely where the heat constraint binds hardest. The overlap has a double significance: it links the estimated response function to the design of climate-adaptive land management [32], and it connects this study to the evidence on how climate and land use jointly shape grain production [63,64].

To test whether the classification is robust, weather-warning records are introduced as an independent check. The records are issued by the National Early Warning Information Release Centre on a basis entirely independent of the gridded temperature product used to construct exposure. The priority counties received about three-quarters more heat warnings per county-year than other counties, and the correlation between county-mean extreme degree days and county-mean heat warnings is 0.42. Once the lightning warnings

that are relatively frequent in the western highlands are set aside, the areas of frequent meteorological warnings coincide broadly with the high-heat grain-producing areas identified here. Because two fully independent data sources point to the same spatial pattern, the identification of high-heat grain-producing areas is confirmed from an independent source. Two cautions follow from the way the classification is built. It rests on county means, so measurement error can move a county across a class boundary, and the warning check spans only 2021–2024, while warning counts reflect administrative practice as well as hazards. The classification is therefore best read as a screening device that indicates where detailed assessment is warranted, not as a ranking of investment priorities, and siting decisions still require field verification.

4. Discussion

Cropland is the part of the land surface where climate variability is converted most directly into grain output, and the humid croplands of southern China and monsoon Asia, which are increasingly exposed to heat damage, are the object of this study. Drawing on a panel of 183 county-level land units in the Sichuan Basin over 2014–2024, the analysis set out to settle three questions: whether heat damages grain production directly in a humid system or only through water deficit; where the damage threshold lies; and where in the basin it matters most. Heat is found to be an important biophysical constraint on grain production in the basin, and that constraint can be located at a specific temperature, a specific month, and a specific part of the basin, while the responses most commonly proposed for it, irrigation among them, cannot fully relax it.

These results agree with the established finding that the temperature–yield relationship is nonlinear and that damage accelerates above a threshold [13,21], as well as with the evidence that extreme heat depresses aggregate agricultural output [19,28]. They differ in three respects. The threshold is located in a humid system where water is not the binding constraint, so the damage cannot be attributed to water deficit, which is where the earlier literature has concentrated [11,14]. Irrigation does not moderate the damage here, whereas in dryland settings from which the temperature–yield literature emerged, it appears effective [11,62]. Furthermore, the negative yield effect is largely offset by an expansion of the sown area, so that total output is statistically unchanged, whereas most studies read yield elasticities as production effects [10]. The discussion that follows therefore turns on five points, namely the temperature threshold, spatial targeting, the July window, the repositioning of irrigation, and the land-use feedback, before setting out the limitations of the analysis. It should be emphasised that what is identified here is a biophysical constraint and its spatial distribution rather than a causal policy effect, so that the management implications are judgements about the location, the severity, and the spatial priority of the constraint, not estimates of the effect of any particular policy instrument.

4.1. EDD30 as a Land–Climate Stress Threshold

The shape of the response function is itself informative, since the constraint on grain production does not appear suddenly but stays flat below about 28 °C, declines slowly through the low thirties, and deepens abruptly above 34 °C; the same graded structure, with thresholds that shift across regions and growth stages, has now been documented for several cereal systems [31,50]. Because yield is measured per sown hectare, losses that operate through a lower harvestable fraction or through failed establishment are not captured, and estimates based on yield alone may understate the production effect of extreme heat [65]. The spatial autocorrelation reported in Section 3.3 is likewise a property that depends on the spatial weights chosen, as is the case for the Moran coefficient

generally [61]. The daily mean temperature of 30 °C that locates this constraint falls in the middle of the 29–34 °C range used in the crop-yield literature [13], and agrees with the agronomic evidence on heat-induced spikelet sterility in rice and on kernel set in maize [7,8]; in this region, it corresponds to a daily maximum of about 34.5 °C, so the estimates obtained here can be compared directly with studies that measure exposure from daily maxima. For land evaluation, this correspondence means that the threshold can be cited without a prior conversion, although the conversion itself is approximate and should be used only for comparison rather than to reconstruct the exposure variable.

Because damage deepens monotonically as the threshold is raised, as Table 4 shows, heat is better understood as a graded constraint than as a single threshold value. Two consequences follow. On the one hand, any threshold that enters a land evaluation embeds a judgement about severity, and the higher the threshold the stricter the risk judgement it expresses; on the other hand, reducing heat risk to a binary constraint, or replacing exposure with annual mean temperature, distorts both the location and the severity of the constraint. That cooling and heating degree days on an 18 °C base, annual mean temperatures, and percentile exceedance days all fail to carry information about crop heat damage is therefore a direct warning against the coarse climatic indices used in land suitability mapping [32]. It should be acknowledged, however, that the EDD32 and EDD34 estimates rest mainly on the record years, so they are better treated as evidence of a severity gradient than as cross-year threshold estimates.

For land-system science, the most appropriate use of this threshold is as a biophysical modifier that enters land capability, land suitability, and land carrying-capacity assessments alongside soil, slope, and drainage variables [9,32], rather than as an agro-economic parameter. The distinction matters because a modifier changes the production ceiling of a given parcel under a given set of management inputs, whereas a parameter directly yields a comparison of returns across inputs; conflating the two risks turning a judgement about heat limitation into a conclusion about investment priorities. For that reason, the threshold identified here is better used to screen the parcels and periods that require further assessment than to substitute for local agronomic trials and engineering appraisal.

4.2. Spatial Targeting of Adaptive Land Management

Viewed spatially, the most immediately usable result is the classification in Figure 6, which sets out a priority class of counties that combine above-median heat exposure with above-median output while the low-heat and low-output, low-heat and high-output, and high-heat and low-output classes absorb the remaining counties. Heat exposure and grain production are therefore not independent of one another but concentrate in the same counties; more importantly, that concentration takes the form of a contiguous block in the eastern basin rather than a scatter of isolated hotspots, echoing the spatial heterogeneity documented for Chinese crop–climate responses more generally [66].

Contiguity determines the scale at which adaptation can be organised. Where the constraint appears as a contiguous land system, whether as an irrigation district, a cropping belt, or a prefectural jurisdiction, denser heat forecasting, the diffusion of substitute cultivars, and the coordination of sowing-date adjustments can be arranged within those units at once [63], instead of being pursued county by county; conversely, allocating resources by administrative level or by total cropland area would place a considerable share of the budget outside the block. In this sense, the paper offers a judgement about where the constraint lies rather than a recommendation about how much to invest.

The reliability of such a spatial judgement depends on the quality of the county-level measures of exposure and output. Measurement error may shift the boundaries of the classes or change the number of priority counties, so the classification should be

re-estimated as the data are updated and cross-checked against independent sources; the warning records used here are one such check, and they show that the priority counties receive markedly more heat warnings and that county-mean extreme degree days and county-mean heat warnings are moderately positively correlated. Even so, the check is best read as a further confirmation of the location of the constraint rather than as an estimate of the effect of any targeting instrument.

The classification also speaks to instruments that already exist. Because the priority class is contiguous, it maps onto the spatial units used for high-standard farmland construction and land consolidation, an instrument with documented effects on grain production [67], and it follows the same spatial logic as prioritisation exercises for land and water management under climate change [46]: it can also inform the zoning of heat-tolerant cultivars, the direction of seed and machinery subsidies, the design of insurance products whose payouts are triggered by accumulated heat, and the ranking of irrigation investment. What is offered here is a judgement about where such instruments would act on the binding constraint, not a comparison of their cost-effectiveness, which would require cost data that the analysis does not contain.

Table 9 collects the measures that follow from the estimates, together with the area and the timing at which each would act, the evidence in this paper that supports it, and the conditions under which it would be inappropriate or unproven.

Table 9. Recommended measures for climate-adaptive land management in the Sichuan Basin, listed in the order in which they can be acted on.

Measure	Where It Applies	Timing	Evidence in This Paper	Condition or Caveat
Adjust the sowing window so that heading and early grain filling avoid the hottest weeks	Priority counties in the eastern basin plain	Before and at sowing, adjusted annually	July carries marginal damage while May, June, and September cannot be distinguished from zero (Table 7)	Constrained by the maturity of the cultivars in the rotation and by labour and machinery scheduling
Shift to earlier-maturing or heat-tolerant cultivars	Priority counties, and wherever heading falls in July	Medium term, at variety renewal	Damage is concentrated at heading and early grain filling, above a daily mean of 30 °C	County-level data on varietal adoption are unavailable, so the targeting is indicative
Concentrate high-standard farmland construction and land consolidation	The contiguous priority block of 67 counties	Multi-year investment cycle	A total of 67 of 177 counties combine above-median exposure with above-median output and produce 69.6% of basin grain	The classification is a median split and should be re-estimated as the data are updated
Re-position irrigation towards reliability during heat waves rather than expansion of area	Basin-wide, where the irrigated share already reaches about 54%	Operational and seasonal	Irrigation does not moderate heat damage, including in dry years (Tables 7 and 8)	Irrigation remains justified by drought risk, and the analysis does not measure supply reliability directly
Trigger insurance payouts and advisories on accumulated heat rather than on mean temperature	Priority counties, with warning records as an external check	Within season	EDD30s carry the damage signal whereas mean temperature and coarse indices carry none (Tables 3 and 4)	Requires a payout trigger definition and a dense station network

Table 9. *Cont.*

Measure	Where It Applies	Timing	Evidence in This Paper	Condition or Caveat
Use the 30 °C threshold as a biophysical modifier in land suitability and capability assessment	Humid cropland of the basin, and humid systems more generally	Medium term, in planning cycles	Damage deepens from 2.52% to 10.23% per 100 degree-days as the base rises from 30 to 34 °C, while CDD18s, HDD18s, mean temperatures, and percentile day counts carry no signal (Table 4)	Calibrated to the daily mean temperature, about 34.5 °C in daily maximum terms

Notes: The measures follow from the estimated location of the constraint rather than from a cost–benefit comparison; the analysis identifies where a measure would act on the binding constraint, not which measure is the most cost-effective.

4.3. Cropping Structure and the July Window

The monthly results place the constraint in July rather than across the whole summer, since July carries a coefficient about six times that of August when the months enter separately, and since the August coefficient collapses to zero when July and August enter jointly while the July coefficient retains its full magnitude. Set against the cropping calendar of the basin, in which rapeseed is harvested in May and rice and maize fill grain in July and August, this identifies which cropping sequences are exposed: those that place heading, tasselling, and early grain filling in July, the phenological window in which the crop is most sensitive to heat. Because the mass of exposure falls in August whereas the marginal damage is carried by July, the mismatch between the two shows that damage depends not on how much heat accumulates but on where in the season it falls.

The management implication is therefore about timing rather than about consequences. Shifting sowing dates so that the sensitive stage avoids the hottest part of July, substituting cultivars with shorter or differently timed phenology, and spreading risk across stages through relay and intercropping all act on the timing of exposure rather than on its biophysical effect [14,25], and the association between cropping-structure adjustment and yield in Chinese grain systems provides supporting evidence for interventions of this kind [64]. Because such decisions, although taken at the field and farm level, are constrained by county-level water allocation, seed supply, and extension services, they are better understood as land-system interventions than as farm-level technical choices [68,69].

The timing evidence also has diagnostic value, since the advancement of flowering that warming commonly induces may move the sensitive stage into, rather than out of, the July window, converting a moderate mean warming into a disproportionate increase in heat exposure at the critical stage. Land-management planning should therefore treat phenological timing as a variable that can be adjusted rather than as a fixed calendar. As before, what is offered here is a direction of management derived from the location of the constraint, not an estimate of the effect of any particular cultivar or sowing-date regime.

4.4. Irrigation: Re-Positioning Rather than Expansion

Where the most familiar management response is concerned, the result is negative: the interaction between EDD30s and the high-irrigation county dummy is small and insignificant, the implied slopes per 100 degree-days in high-irrigation and low-irrigation counties are each precisely estimated, and the two are statistically indistinguishable, so that the absence of moderation is more likely to be a genuine null than a matter of insufficient power in one group. By contrast, the interaction between EDD30s and the historically hot county dummy is likewise insignificant, which indicates that past exposure does not alter the marginal damage. Splitting the EDD30 slope between the two record years and the

remaining years gives −3.30% and −6.76% per 100 degree-days respectively, a difference that is not statistically significant, so the marginal damage per degree-day is no larger in the record years; what sets those years apart is how much heat accumulated rather than how damaging each degree-day was.

The result is not unique to this basin. In the monsoon plains of South Asia, irrigation has been shown to have little influence on pre-monsoon heat stress [70], and where the two pathways have been separated with satellite data, irrigation alleviates water stress far more than it alleviates heat stress [71]. In a humid climate with adequate rainfall, irrigation confers little protection against warming [72]. The null does not imply that irrigation is worthless. It implies that, in a basin whose irrigated share is already high, extending the irrigated area has limited marginal value for heat, and that its justification should rest on drought risk rather than on heat risk. The emphasis of irrigation policy is better placed on the reliability of supply during a heat wave than on the extent of irrigated area. Conflating the two would misdirect a substantial share of agricultural infrastructure investment. The counties with the greatest heat exposure are not necessarily those with the most variable rainfall, and irrigation cannot alter the direct thermal load borne by the crop canopy [11,62]. The point also helps to explain why the relationship between heat and water deficit matters so much: in dry regions where the temperature–yield literature was first developed, the two are strongly collinear and the protective role of irrigation appears self-evident, whereas in a humid basin where they are decoupled, that protection disappears. The reason is mechanical. In a dry setting, irrigation raises soil moisture and lowers canopy temperature through transpiration, substituting for rainfall that is absent in the hot season; heat stress and water stress are then two faces of the same deficit, so that applying water addresses both at once. In a humid basin, the crop is not water-limited in most years, and water applied during a heat wave cannot reduce the atmospheric and radiative heat load borne by the canopy. Policy transfer fails precisely where the climatic context changes: an intervention validated in dryland systems should not be assumed to work in humid ones, and the instruments that do act on this constraint, namely the cropping calendar, cultivar phenology, and cropping structure, have no counterpart in the dryland toolkit.

Two qualifications are in order. First, the irrigation variable is the irrigated share of cropland, which measures the extent of irrigation rather than the reliability of supply during a heat wave, and a system that is nominally irrigated but supply-constrained in a dry year will not buffer heat. Second, the basin on which the estimates rest already has a mean irrigated share of 54%, so that what is observed is the effect of variation around a high level, and the conclusion should not be extrapolated to regions where irrigation is currently minimal. In addition, the interaction between irrigation and measures such as cultivar choice or sowing date is not identified in these data, which is a natural direction for further work.

4.5. Land-Use Feedback and the Interpretation of Yield Losses

Once the yield effect is decomposed into a land-use component and an output component, a result emerges that is easy to overlook but important for policy: heat lowers yield per hectare while modestly expanding sown area, so that the net effect on total grain output is statistically indistinguishable from zero. Reading a yield elasticity as a production elasticity would therefore overstate the food-security exposure of the basin, while an analysis confined to yield would miss the response that farmers actually make, which belongs to the land system rather than to agronomy [10]. That response is statistically identifiable but economically small, so the muted output effect is more plausibly the arithmetic consequence of offsetting yield and area effects than evidence of deliberate adaptation.

Such an offset is not costless. Where cropland is limited, area expansion can only come from reduced fallow, a higher multiple-cropping index, or from the cultivation of more marginal land, and each of these paths carries different consequences for soil quality, input use, and long-run productivity [53,64,73] while potentially competing with conservation and carbon objectives [16,17]. Whether the compensatory expansion is sustainable is therefore a question about land-system dynamics that the present data cannot answer, since it depends on the interaction between soil fertility, water rights, labour opportunities, and policy constraints over longer periods rather than on anything the yield equation itself can capture.

Methodologically, what this result does establish is comparatively firm: the land-use margin is an active part of the response to climate stress rather than a fixed background condition. Land-system models that hold area constant will misestimate climate impacts on production, and the same applies to assessments built on simulated rather than observed land use [40] and work linking cropland expansion to temperature extremes [74]. The direction that follows is a framework in which area, yield, and inputs are jointly endogenous, rather than one more elasticity estimate.

Several limitations bound these readings. Exposure is measured from the daily mean rather than daily maximum temperature, and ERA5-Land underestimates temperature in complex terrain [48]; the high-threshold estimates rest mainly on the record years, since EDD32s and EDD34s have thin support; the rural-economy variables for 2016 duplicate those of 2015 because of a mis-labelled yearbook table, so a 2017–2024 subsample is reported alongside the baseline; and the residual spatial autocorrelation is accommodated with Conley spatial HAC standard errors rather than modelled. The mechanism evidence also remains indirect, since the monthly profile identifies when the constraint binds rather than why. Relaxing these limits would require a parallel specification on the daily maximum temperature, county-level phenological and radiation observations, and farm-level data on adaptation.

5. Conclusions

In the humid Sichuan Basin, where heat and water deficit are decoupled, extreme heat is a binding biophysical constraint on grain production and operates through a direct thermal channel rather than through water deficit. The analysis locates that constraint at a specific temperature, a specific month, and a specific part of the basin. It draws on a panel of 183 county-level land units over 2014–2024, of which 177 enter the estimation sample, and separates moderate warmth from extreme heat by construction rather than by statistical adjustment. Over the July–August critical growth period, an additional 100 growing degree days raises the grain yield by 2.70%, whereas an additional 100 extreme degree days above 30 °C lowers it by 3.24%. The constraint is graded rather than threshold-like, since, over the annual window reported in Table 4, damage deepens from 2.52% per 100 degree-days at a 30 °C base to 10.23% at 34 °C. It is also specific rather than general, because cooling and heating degree days on an 18 °C base, the annual mean temperature, and percentile exceedance days carry no information about crop heat damage at all. Damage is concentrated in July, when heading, tasselling, and early grain filling coincide with the hottest weeks of the year. It is equally concentrated in space, since 67 of the 177 estimation counties combine above-median heat exposure with above-median output and account for 69.6% of basin grain.

Read together, these results support that reading, and because the two candidate channels are decoupled rather than collinear in a humid setting, the inference is eliminative rather than a direct identification of the mechanism, since the data cannot separate them. Where heat and water stress have been separated for maize in the United States, heat rather

than water dominates the effect on yield stability [75]. The heat coefficient is unchanged by prefecture-level clustering, remains significant under Conley spatial HAC inference at every bandwidth tested, and keeps its sign and significance in every specification tested, although its magnitude varies with the sample: it reaches −8.59% per 100 degree-days when 2022 is excluded and −1.15% in the 2017–2024 subsample, against −3.24% in the full sample. The width of that range reflects how concentrated extreme heat is in a small number of hot years rather than any fragility in the sign of the effect. Therefore, the short-range spatial autocorrelation that the residuals retain is measured and accommodated rather than assumed away. Irrigation does not moderate the damage, and the negative yield effect is partly offset by an expansion of the sown area, which leaves total grain output statistically unchanged. The constraint is thus real and spatially located. The land-use margin responds statistically but only weakly, so yield losses are not fully offset by area expansion, and the most familiar management response does not relax the constraint.

The management reading is correspondingly specific, although it concerns the location, severity, and spatial priority of a biophysical constraint rather than the estimated effect of any policy instrument. Because the damage is concentrated in July, the levers that act on the timing of exposure, namely sowing dates, cultivar phenology, and cropping structure, are better matched to it than irrigation is. Because irrigation does not moderate heat damage in this humid setting, its justification should rest on drought risk rather than on heat risk. If adaptation resources are to be concentrated rather than spread evenly, the contiguous eastern plain is where the returns are highest, since close to two-thirds of basin grain is produced there under the strongest heat constraint. Together, the results support adjusting cropping calendars and cultivar choice rather than expanding irrigation, targeting climate-adaptive land management on the eastern basin plain, and treating the land-use margin as part of the response to heat rather than a fixed background condition. Whether the direct thermal channel also dominates in other humid subtropical and monsoon croplands remains an open question, and the framework developed here can be transferred to those settings without assuming that it does.

Supplementary Materials: The following supporting information can be downloaded at: https://www.mdpi.com/article/10.3390/land15101974/s1.

Author Contributions: Conceptualisation, X.L. and Y.Q.; methodology, X.L. and Q.H.; formal analysis, X.L.; data curation, X.L.; writing of the original draft, X.L.; review and editing, Y.Q.; supervision, Y.Q. All authors have read and agreed to the published version of the manuscript.

Funding: This research received no external funding.

Data Availability Statement: Publicly available source datasets can be accessed through the providers listed in Table 1. The derived county panel, the Stata replication code, and the analysis outputs supporting the findings of this study can be obtained from the corresponding author upon reasonable request. Redistribution of some source datasets may be subject to the terms of use of the original providers.

Acknowledgments: The authors thank colleagues at the College of Economics, Sichuan Agricultural University, for comments on an earlier draft, and acknowledge the providers of the gridded temperature and ERA5-Land reanalysis products used in this study. Jiang Qiurui and Li Nianci are thanked for assistance with data collection.

Conflicts of Interest: The authors declare no conflicts of interest.

References

1. Wheeler, T.; von Braun, J. Climate Change Impacts on Global Food Security. *Science* **2013**, *341*, 508–513. [CrossRef]

2. Lesk, C.; Rowhani, P.; Ramankutty, N. Influence of extreme weather disasters on global crop production. *Nature* **2016**, *529*, 84–87. [CrossRef]
3. Pörtner, H.-O.; Scholes, R.J.; Arneth, A.; Barnes, D.K.A.; Burrows, M.T.; Diamond, S.E.; Duarte, C.M.; Kiessling, W.; Leadley, P.; Managi, S.; et al. Overcoming the coupled climate and biodiversity crises and their societal impacts. *Science* **2023**, *380*, eabl4881. [CrossRef]
4. Liu, Y.; Yuan, S.; Zhu, Y.; Ren, L.; Chen, R.; Zhu, X.; Xia, R. The patterns, magnitude, and drivers of unprecedented 2022 mega-drought in the Yangtze River Basin, China. *Environ. Res. Lett.* **2023**, *18*, 114006. [CrossRef]
5. Pongratz, J.; Schwingshackl, C.; Bultan, S.; Obermeier, W.; Havermann, F.; Guo, S. Land Use Effects on Climate: Current State, Recent Progress, and Emerging Topics. *Curr. Clim. Change Rep.* **2021**, *7*, 99–120. [CrossRef]
6. Lobell, D.B.; Gourdji, S.M. The Influence of Climate Change on Global Crop Productivity. *Plant Physiol.* **2012**, *160*, 1686–1697. [CrossRef]
7. Peng, S.; Huang, J.; Sheehy, J.E.; Laza, R.C.; Visperas, R.M.; Zhong, X.; Centeno, G.S.; Khush, G.S.; Cassman, K.G. Rice yields decline with higher night temperature from global warming. *Proc. Natl. Acad. Sci. USA* **2004**, *101*, 9971–9975. [CrossRef]
8. Welch, J.R.; Vincent, J.R.; Auffhammer, M.; Moya, P.F.; Dobermann, A.; Dawe, D. Rice yields in tropical/subtropical Asia exhibit large but opposing sensitivities to minimum and maximum temperatures. *Proc. Natl. Acad. Sci. USA* **2010**, *107*, 14562–14567. [CrossRef]
9. Verburg, P.H.; Crossman, N.; Ellis, E.C.; Heinimann, A.; Hostert, P.; Mertz, O.; Nagendra, H.; Sikor, T.; Erb, K.-H.; Golubiewski, N.; et al. Land system science and sustainable development of the earth system: A global land project perspective. *Anthropocene* **2015**, *12*, 29–41. [CrossRef]
10. Meyfroidt, P.; de Bremond, A.; Ryan, C.M.; Archer, E.; Aspinall, R.; Chhabra, A.; Camara, G.; Corbera, E.; DeFries, R.; Díaz, S.; et al. Ten facts about land systems for sustainability. *Proc. Natl. Acad. Sci. USA* **2022**, *119*, e2109217118. [CrossRef]
11. Troy, T.J.; Kipgen, C.; Pal, I. The impact of climate extremes and irrigation on US crop yields. *Environ. Res. Lett.* **2015**, *10*, 054013. [CrossRef]
12. Kirk, N.A.; Cradock-Henry, N.A. Land Management Change as Adaptation to Climate and Other Stressors: A Systematic Review of Decision Contexts Using Values-Rules-Knowledge. *Land* **2022**, *11*, 791. [CrossRef]
13. Schlenker, W.; Roberts, M.J. Nonlinear temperature effects indicate severe damages to U.S. crop yields under climate change. *Proc. Natl. Acad. Sci. USA* **2009**, *106*, 15594–15598. [CrossRef]
14. Lobell, D.B.; Bänziger, M.; Magorokosho, C.; Vivek, B. Nonlinear heat effects on African maize as evidenced by historical yield trials. *Nat. Clim. Change* **2011**, *1*, 42–45. [CrossRef]
15. Lesk, C.; Coffel, E.; Winter, J.; Ray, D.; Zscheischler, J.; Seneviratne, S.I.; Horton, R. Stronger temperature–moisture couplings exacerbate the impact of climate warming on global crop yields. *Nat. Food* **2021**, *2*, 683–691. [CrossRef]
16. Bayer, A.D.; Lautenbach, S.; Arneth, A. Benefits and trade-offs of optimizing global land use for food, water, and carbon. *Proc. Natl. Acad. Sci. USA* **2023**, *120*, e2220371120. [CrossRef]
17. Power, A.G. Ecosystem services and agriculture: Tradeoffs and synergies. *Philos. Trans. R. Soc. B Biol. Sci.* **2010**, *365*, 2959–2971. [CrossRef]
18. Sun, R.; Ye, T.; Liu, Y.; Liu, W.; Chen, S. Spatiotemporal variation of growth-stage specific concurrent climate extremes and their impacts on rice yield in southern China. *Earth Syst. Dyn.* **2025**, *16*, 1971–1988. [CrossRef]
19. Burke, M.; Hsiang, S.M.; Miguel, E. Global non-linear effect of temperature on economic production. *Nature* **2015**, *527*, 235–239. [CrossRef]
20. Roberts, M.J.; Schlenker, W.; Eyer, J. Agronomic Weather Measures in Econometric Models of Crop Yield with Implications for Climate Change. *Am. J. Agric. Econ.* **2012**, *95*, 236–243. [CrossRef]
21. Zhao, C.; Liu, B.; Piao, S.; Wang, X.; Lobell, D.B.; Huang, Y.; Huang, M.; Yao, Y.; Bassu, S.; Ciais, P.; et al. Temperature increase reduces global yields of major crops in four independent estimates. *Proc. Natl. Acad. Sci. USA* **2017**, *114*, 9326–9331. [CrossRef]
22. Asseng, S.; Ewert, F.; Martre, P.; Rötter, R.P.; Lobell, D.B.; Cammarano, D.; Kimball, B.A.; Ottman, M.J.; Wall, G.W.; White, J.W.; et al. Rising temperatures reduce global wheat production. *Nat. Clim. Change* **2014**, *5*, 143–147. [CrossRef]
23. Lobell, D.B.; Schlenker, W.; Costa-Roberts, J. Climate Trends and Global Crop Production Since 1980. *Science* **2011**, *333*, 616–620. [CrossRef]
24. Deng, Q.; Xie, W.; Wang, K. Impact of extreme temperatures on production of different rice types: A county-level analysis for China. *Appl. Econ. Perspect. Policy* **2022**, *45*, 1097–1133. [CrossRef]
25. Deschênes, O.; Greenstone, M. The Economic Impacts of Climate Change: Evidence from Agricultural Output and Random Fluctuations in Weather. *Am. Econ. Rev.* **2007**, *97*, 354–385. [CrossRef]
26. Dell, M.; Jones, B.F.; Olken, B.A. Temperature Shocks and Economic Growth: Evidence from the Last Half Century. *Am. Econ. J. Macroecon.* **2012**, *4*, 66–95. [CrossRef]
27. Hsiang, S.M.; Burke, M.; Miguel, E. Quantifying the Influence of Climate on Human Conflict. *Science* **2013**, *341*, 1235367. [CrossRef]

28. Carter, C.; Cui, X.; Ghanem, D.; Mérel, P. Identifying the Economic Impacts of Climate Change on Agriculture. *Annu. Rev. Resour. Econ.* **2018**, *10*, 361–380. [CrossRef]
29. Conley, T.G. GMM estimation with cross sectional dependence. *J. Econom.* **1999**, *92*, 1–45. [CrossRef]
30. Cameron, A.C.; Miller, D.L. A Practitioner's Guide to Cluster-Robust Inference. *J. Hum. Resour.* **2015**, *50*, 317–372. [CrossRef]
31. Zhao, Q.; Wang, C.; Wang, X.; Rezaei, E.E.; Müller, C.; Wang, E.; Webber, H.; Zhang, L.; Li, X.; Sang, Y.; et al. Temperature thresholds of extreme heat-induced yield loss in maize and soybean reveal geographic heterogeneity across the Northern Hemisphere. *Nat. Food* **2026**, *7*, 194–205. [CrossRef]
32. Abadie, A.; Athey, S.; Imbens, G.W.; Wooldridge, J.M. When Should You Adjust Standard Errors for Clustering? *Q. J. Econ.* **2022**, *138*, 1–35. [CrossRef]
33. Huang, X.; Zhang, T.; Jiang, X.; Liu, S.; Xiao, D. Interannual variability of mid-summer heat wave frequency over the Sichuan Basin. *Int. J. Climatol.* **2021**, *41*, 5036–5050. [CrossRef]
34. Critchley, W.; Harari, N.; Mollee, E.; Mekdaschi-Studer, R.; Eichenberger, J. Sustainable Land Management and Climate Change Adaptation for Small-Scale Land Users in Sub-Saharan Africa. *Land* **2023**, *12*, 1206. [CrossRef]
35. Hurlbert, M.; Meghdadi, H.; Fletcher, A.J.; Hillis, E.; Barman, P.R.D.; Ezra, A.; Finlay, K. Compound Climate Events: Adaptation to Agricultural Drought and Flood on the Prairies of Saskatchewan, Canada. *Land* **2026**, *15*, 1592. [CrossRef]
36. Hsiang, S. Climate Econometrics. *Annu. Rev. Resour. Econ.* **2016**, *8*, 43–75. [CrossRef]
37. Auffhammer, M.; Hsiang, S.M.; Schlenker, W.; Sobel, A. Using Weather Data and Climate Model Output in Economic Analyses of Climate Change. *Rev. Environ. Econ. Policy* **2013**, *7*, 181–198. [CrossRef]
38. Moran, P.A.P. Notes on continuous stochastic phenomena. *Biometrika* **1950**, *37*, 17–23. [CrossRef]
39. Anselin, L. Local Indicators of Spatial Association–LISA. *Geogr. Anal.* **1995**, *27*, 93–115. [CrossRef]
40. Cao, X.; Han, J.; Li, X. Analysis of the Impact of Land Use Change on Grain Production in Jiangsu Province, China. *Land* **2023**, *13*, 20. [CrossRef]
41. Turner, B.L.; Lambin, E.F.; Reenberg, A. The emergence of land change science for global environmental change and sustainability. *Proc. Natl. Acad. Sci. USA* **2007**, *104*, 20666–20671. [CrossRef]
42. Foley, J.A.; DeFries, R.; Asner, G.P.; Barford, C.; Bonan, G.; Carpenter, S.R.; Chapin, F.S.; Coe, M.T.; Daily, G.C.; Gibbs, H.K.; et al. Global Consequences of Land Use. *Science* **2005**, *309*, 570–574. [CrossRef]
43. Liu, J.; Shen, W.; He, Y. Effects of Cropland Expansion on Temperature Extremes in Western India from 1982 to 2015. *Land* **2021**, *10*, 489. [CrossRef]
44. Chen, S.; Chen, X.; Xu, J. Impacts of climate change on agriculture: Evidence from China. *J. Environ. Econ. Manag.* **2016**, *76*, 105–124. [CrossRef]
45. Cui, X.; Zhong, Z. Climate change, cropland adjustments, and food security: Evidence from China. *J. Dev. Econ.* **2024**, *167*, 103245. [CrossRef]
46. Zagaria, C.; Schulp, C.J.; Malek, Ž.; Verburg, P.H. Potential for land and water management adaptations in Mediterranean croplands under climate change. *Agric. Syst.* **2023**, *205*, 103586. [CrossRef]
47. Kassie, B.T.; Van Ittersum, M.K.; Hengsdijk, H.; Asseng, S.; Wolf, J.; Rötter, R.P. Climate-induced yield variability and yield gaps of maize (Zea mays L.) in the Central Rift Valley of Ethiopia. *Field Crops Res.* **2014**, *160*, 41–53. [CrossRef]
48. Zabel, F.; Putzenlechner, B.; Mauser, W. Global Agricultural Land Resources–A High Resolution Suitability Evaluation and Its Perspectives until 2100 under Climate Change Conditions. *PLoS ONE* **2014**, *9*, e107522. [CrossRef]
49. Sun, T.; Hasegawa, T.; Liu, B.; Tang, L.; Liu, L.; Cao, W.; Zhu, Y. Current rice models underestimate yield losses from short-term heat stresses. *Glob. Chang. Biol.* **2021**, *27*, 402–416. [CrossRef]
50. Liu, Z.; Cammarano, D.; Liu, X.; Tian, Y.; Zhu, Y.; Cao, W.; Cao, Q. Winter wheat yield responses to growing degree days: Long-term trends and adaptability in major producing areas of China. *Ecol. Indic.* **2025**, *170*, 113058. [CrossRef]
51. Li, Q.; Wang, P.; Li, Y.; Tang, J.; Li, X.; Zhang, Y.; Han, D.; Zhao, Y.; Wang, Q.; Yang, Z. Identifying trigger thresholds for heat damage at different growth stages of summer maize: A case study of the Huang-Huai-Hai Plain, China. *Eur. J. Agron.* **2025**, *170*, 127729. [CrossRef]
52. Jiang, T.; He, L.; Feng, H.; He, J.; Yu, Q. Understanding the impacts of extreme temperature and humidity compounds on winter wheat traits in China. *Agric. For. Meteorol.* **2025**, *362*, 110354. [CrossRef]
53. He, D.; Wang, J.; Dai, T.; Feng, L.; Zhang, J.; Pan, X.; Pan, Z. Impact of climate change on maize potential productivity and the potential productivity gap in southwest China. *J. Meteorol. Res.* **2014**, *28*, 1155–1167. [CrossRef]
54. Wang, P.; Zhang, Z.; Chen, Y.; Wei, X.; Feng, B.; Tao, F. How much yield loss has been caused by extreme temperature stress to the irrigated rice production in China? *Clim. Change* **2016**, *134*, 635–650. [CrossRef]
55. Shi, X.; Zhu, W. Spatio-temporal patterns and drivers of irrigation water requirement in mainland China. *Agric. Water Manag.* **2025**, *308*, 109283. [CrossRef]
56. Xiong, W.; Holman, I.P.; You, L.; Yang, J.; Wu, W. Impacts of observed growing-season warming trends since 1980 on crop yields in China. *Reg. Environ. Change* **2014**, *14*, 7–16. [CrossRef]

57. Ojo, T.O.; Baiyegunhi, L.J.S. Determinants of climate change adaptation strategies and its impact on the net farm income of rice farmers in south-west Nigeria. *Land Use Policy* **2020**, *95*, 103946. [CrossRef]
58. Colella, F.; Lalive, R.; Sakalli, S.O.; Thoenig, M. acreg: Arbitrary correlation regression. *Stata J.* **2023**, *23*, 119–147. [CrossRef]
59. Pan, T.; Du, G.; Dong, J.; Kuang, W.; De Maeyer, P.; Kurban, A. Divergent changes in cropping patterns and their effects on grain production under different agro-ecosystems over high latitudes in China. *Sci. Total Environ.* **2019**, *659*, 314–325. [CrossRef]
60. Zhi, J.; Cao, X.; Zhang, Z.; Qin, T.; Qu, L.; Qi, L.; Ge, L.; Guo, A.; Wang, X.; Da, C.; et al. Identifying the determinants of crop yields in China since 1952 and its policy implications. *Agric. For. Meteorol.* **2022**, *327*, 109216. [CrossRef]
61. Griffith, D.A.; Chun, Y. Some useful details about the Moran coefficient, the Geary ratio, and the join count indices of spatial autocorrelation. *J. Spat. Econom.* **2022**, *3*, 12. [CrossRef]
62. Meng, M.; Yu, L.; Yu, X. Machinery structure, machinery subsidies, and agricultural productivity: Evidence from China. *Agric. Econ.* **2024**, *55*, 223–246. [CrossRef]
63. Ortiz-Bobea, A.; Ault, T.R.; Carrillo, C.M.; Chambers, R.G.; Lobell, D.B. Anthropogenic climate change has slowed global agricultural productivity growth. *Nat. Clim. Change* **2021**, *11*, 306–312. [CrossRef]
64. Luo, M.; Lau, N.-C. Heat Waves in Southern China: Synoptic Behavior, Long-Term Change, and Urbanization Effects. *J. Clim.* **2017**, *30*, 703–720. [CrossRef]
65. Xiao, K.; Zhou, X.; Gui, H.; Tian, Y.; Chen, X.; Li, Y.; Matomela, N.; Xin, Q. Drought and extreme heat reduce wheat and maize production in the United States by lowering both crop yields and harvestable fraction. *Earth's Future* **2025**, *13*, e2024EF005557. [CrossRef]
66. Liu, C.-J.; Li, X.-Y.; Chamberlin, J.; You, L.-Z. Climate change-induced northward shifts in double cropping system in China: Implications for crop production potential and water use. *Adv. Clim. Chang. Res.* **2025**, *16*, 1239–1249. [CrossRef]
67. Hao, S.; Wang, G.; Yang, Y.; Zhao, S.; Huang, S.; Liu, L.; Zhang, H. Promoting grain production through high-standard farmland construction: Evidence in China. *J. Integr. Agric.* **2024**, *23*, 324–335. [CrossRef]
68. Zhang, X.; Ma, X. Misplaced optimism in agricultural land usage driven by newly available climate resources: A case study of estimated and realized cropping intensity in northern and northeastern China. *Clim. Risk Manag.* **2019**, *25*, 100194. [CrossRef]
69. Zhao, Y.; Xiong, L.; Yin, J.; Zha, X.; Li, W.; Han, Y. Understanding the effects of flash drought on vegetation photosynthesis and potential drivers over China. *Sci. Total Environ.* **2024**, *931*, 172926. [CrossRef]
70. Jha, R.; Mondal, A.; Devanand, A.; Roxy, M.K.; Ghosh, S. Limited influence of irrigation on pre-monsoon heat stress in the Indo-Gangetic Plain. *Nat. Commun.* **2022**, *13*, 4275. [CrossRef]
71. Zhu, P.; Burney, J. Untangling irrigation effects on maize water and heat stress alleviation using satellite data. *Hydrol. Earth Syst. Sci.* **2022**, *26*, 827–840. [CrossRef]
72. Anapalli, S.S.; Pinnamaneni, S.R.; Fisher, D.K.; Reddy, K.N. Vulnerabilities of irrigated and rainfed corn to climate change in a humid climate in the Lower Mississippi Delta. *Clim. Change* **2021**, *164*, 5. [CrossRef]
73. Ma, L.; Wei, Y.; Dong, W. Evaluation and Spatiotemporal Evolution of Surface Air Temperature Estimated by ERA5-Land Reanalysis Data in East China. *J. Appl. Meteorol. Climatol.* **2025**, *64*, 943–958. [CrossRef]
74. National Bureau of Statistics of China. *China Statistical Yearbook 2024*; China Statistics Press: Beijing, China, 2024.
75. Liu, W.; Zhou, J.; Luo, Y.; Chen, S.; Ma, Y. Reduced crop yield stability is more likely to be associated with heat than with moisture extremes in the US Midwest. *Earth's Future* **2025**, *13*, e2024EF005172. [CrossRef]

Disclaimer/Publisher's Note: The statements, opinions and data contained in all publications are solely those of the individual author(s) and contributor(s) and not of MDPI and/or the editor(s). MDPI and/or the editor(s) disclaim responsibility for any injury to people or property resulting from any ideas, methods, instructions or products referred to in the content.